

Robust Multiscale Methods for Helmholtz equations in high contrast heterogeneous media

Xingguang Jin^{a,*}, Changqing Ye^a, Eric T. Chung^a

^a*Department of Mathematics, The Chinese University of Hong Kong, Shatin, Hong Kong SAR.*

Abstract

In this paper, we provide the constraint energy minimization generalized multiscale finite element method (CEM-GMsFEM) to solve Helmholtz equations in heterogeneous medium. This novel multiscale method is specifically designed to overcome problems related to pollution effect, high-contrast coefficients, and the loss of hermiticity of operators. We establish the inf-sup stability and give an a priori error estimate for this method under a number of established assumptions and resolution conditions. The theoretical results are validated by a set of numerical tests, which further show that the multiscale technique can effectively capture pertinent physical phenomena.

Keywords: CEM-GMsFEM, Helmholtz equation, Heterogeneous, Error estimate

1. Introduction

1 The Helmholtz equation models wave propagation and scattering phe-
2 nomena in the frequency domain arising in a variety of science and engineer-
3 ing applications, including seismic imaging that helps to model and analyze
4 how seismic waves propagate through the Earth's subsurface, medical ultra-
5 sound technologies to simulate and understand the behavior of ultrasound
6 waves in human tissues for diagnostic imaging purposes, and underwater
7 acoustics to study the propagation of sound waves in the ocean and predict
8 their behavior for sonar applications, underwater communication, and marine

*Corresponding author.

Email address: xgjin@math.cuhk.edu.hk (Xingguang Jin)

9 research [1, 2]. Designing robust and accurate numerical methods for solving
10 the Helmholtz equation can still be challenging, particularly when dealing
11 with high-wavenumber problems or heterogeneous coefficients [3]. It is well-
12 known that Galerkin Finite element Method (FEM) leads to quasi-optimal
13 error estimates with respect to the degrees of freedoms which is affected by
14 the wavenumber when applied to the Helmholtz equations. As a result, the
15 mesh size should be chosen small enough and also the arising system of lin-
16 ear equations is highly indefinite such that the solution process becomes too
17 expensive for the large wavenumber [4]. The properties of material are usu-
18 ally assumed to have constant density and same speed of sound when study
19 acoustic wave propagation, and for the Helmholtz equations with constant
20 coefficients or low contrast coefficients, pollution effect can be resolved by
21 many well developed and designed approaches such as the partition of unity
22 finite element methods [5], the least squares finite element methods [6], the
23 generalized finite element methods [7], the hybridized discontinuous Galerkin
24 methods [8], the interior penalty discontinuous Galerkin methods [9] and *hp*-
25 FEM [10, 11]. When dealing with complex materials, such as composites,
26 where multiple scales are present within the domain, the challenges become
27 even more significant. In such cases, multiscale methods can be employed
28 to resolve the micro scales and capture the effective behavior of the mate-
29 rial. These methods aim to bridge the gap between the fine-scale details and
30 the macroscopic behavior by incorporating appropriate scale decomposition
31 techniques and coupling strategies.

32 Multiscale methods have long been developed to solve the difficulties as-
33 sociated with the rough coefficients in elliptic equations [12, 13, 14]. A com-
34 monly shared idea of these methods is to encode fine-scale information into
35 the basis functions of finite element methods. Once the fine-scale information
36 is encoded into the basis functions, the original problem can be solved using
37 multiscale finite element spaces. These spaces have reduced dimensions com-
38 pared to the default FEM spaces. The reduction in dimensions is achieved
39 by effectively representing the solution behavior at multiple scales using a
40 smaller set of basis functions. These methods have significantly advanced
41 the field of multiscale computational methods and provided efficient and ac-
42 curate tools for solving problems with multiscale characteristics. These meth-
43 ods have shown promise in capturing the behavior of solutions at different
44 scales and providing accurate approximations in problems with high contrast
45 and heterogeneity. These methods have also been applied to solve Helmholtz
46 equations in heterogeneous domains efficiently, such as Localized Orthogo-

47 nal Decomposition (LOD) [15, 16] method, Super-LOD method [17], Mul-
 48 tiscala Petrov–Galerkin Method [18], Generalized Multiscale Finite Element
 49 methods (GMsFEM) [19], Edge Multiscale Interior Penalty Discontinuous
 50 Galerkin method [20], Multiscale spectral generalized finite element method
 51 [21], Exponentially convergent multiscale methods [22] etc. Recently, a novel
 52 multiscale method named Constraint Energy Minimization Generalized Mul-
 53 tiscala Finite Element Method (CEM-GMsFEM) is initially developed by [23]
 54 which is aimed for the high-contrast problems and it has been successfully
 55 applied to various partial differential equations arising from practical appli-
 56 cations, see, e.g., [24, 25, 26]. This approach and the LOD method have
 57 certain similarities. For instance, they both rely on the exponential decay
 58 features of basis functions and require mesh sizes that are dependent on the
 59 oversampling regions in order to achieve the appropriate convergence rate
 60 [27]. Instead of using quasi-interpolation operators to split the solution into
 61 macroscopic and microscopic components in LOD, we employ element-wise
 62 projections in the implementation of CEM-GMsFEM method, which is the
 63 core idea from GMsFEM [28]. To the best of our knowledge, CEM-GMsFEM
 64 has not been widely explored to solve Heterogeneous Helmholtz equations. In
 65 this paper, we focus on the specific setting of the diffusion coefficients which
 66 take either ε^2 on one part of the domain or a small value on the complement
 67 of the domain due to the fact that the effects observed in time-harmonic
 68 wave propagation can differ depending on whether the diffusion coefficient
 69 is small or not [29, 15]. In the original CEM-GMsFEM, the newly obtained
 70 trial and test spaces of multiscale basis functions are the same; however, be-
 71 cause the Helmholtz equations are inherently indefinite, we take a cue from
 72 the Multiscale Petrov-Galerkin method [30, 18] and form distinct trial and
 73 test multiscale spaces by leveraging standard procedures of CEM-GMsFEM
 74 in order to develop a tailored approach for solving the Helmholtz equation
 75 in such scenarios.

76 The aim of this paper is to explore an efficient method to solve Hetero-
 77 geneous Helmholtz problems by using the novel multiscale model reduction
 78 skills coming from CEM-GMsFEM, which beyond the need of periodic co-
 79 efficients [18] or other requirements of the coefficients structures. In the
 80 analysis section, we establish a resolution condition and build the inf-sup
 81 condition of both global problem and multiscale problem to secure their well-
 82 posedness. Subsequently, the exponential decay properties of basis functions
 83 are demonstrated, and ultimately, we obtain the error estimate of our mul-
 84 tiscala method with the desired the convergence rate. For the first time, we

85 present the evidence supporting of the convergence of CEM-GMsFEM for
86 the Helmholtz equations in heterogeneous media. The numerical simulation
87 section displays the three experiments correspond to three kinds of media,
88 which supports the effectiveness of CEM-GMsFEM and the pollution effect
89 is resolved by using the coarser mesh size to achieve the quasi-optimal con-
90 vergence. We evaluate the relative error of the CEM-GMsFEM method with
91 respect to different coarse mesh sizes and different oversampling layers in ta-
92 bles 2 to 4. The oversampling layers refer to additional layers of elements or
93 degrees of freedom surrounding the coarse mesh, which capture the fine-scale
94 details and improve the accuracy of the approximation. The results of the
95 experiments indicate that the relative errors are influenced by the choice of
96 oversampling layers, which distinguishes the CEM-GMsFEM method from
97 traditional FEM. This suggests that the oversampling layers play a significant
98 role in capturing the fine-scale information and reducing the approximation
99 error. We also compare the relative errors obtained with different oversam-
100 pling layer configurations to demonstrate the impact of these layers on the
101 accuracy of the method.

102 By highlighting the influence of oversampling layers on the relative errors,
103 we emphasize the advantage of the CEM-GMsFEM method over traditional
104 FEM in capturing fine-scale information and improving the accuracy of the
105 solution. This finding further supports the effectiveness and efficiency of the
106 proposed method in solving Helmholtz equations in heterogeneous domains.

107 Our paper is organized as follows. In section 2, we present the weak for-
108 mulations of Helmholtz equations with homogeneous Robin boundary con-
109 ditions as well as introducing the notations of grids. Then in section 3 we
110 construct multiscale basis functions to construct multiscale trial space and
111 multiscale test space of our CEM-GMsFEM respectively. In section 4, we
112 analyze the convergence of CEM-GMsFEM and derive the error estimates.
113 In section 5, some numerical experiments are carried out to demonstrate the
114 proposed theories. Finally, some conclusions can be found in section 6.

115 **2. Preliminaries**

116 We consider the following Helmholtz equation for heterogeneous media
 117 in the bounded space domain $\Omega \subset \mathbb{R}^d$ where $d = 2$ or 3 :

$$\begin{cases} -\nabla \cdot (A\nabla u) - k^2 u = f & \text{in } \Omega, \\ u = 0 & \text{on } \Gamma_D, \\ A\nabla u \cdot \mathbf{n} - ik u = 0 & \text{on } \Gamma_R, \end{cases} \quad (1)$$

118 where $\Gamma = \Gamma_D \cup \Gamma_N \cup \Gamma_R$ is a Lipschitz continuous boundary where $\Gamma_D, \Gamma_N, \Gamma_R$
 119 represents the Dirichlet, Neumann and Robin boundary conditions respec-
 120 tively, \mathbf{n} is the unit outward normal vector to the boundary, $k \in \mathbb{R}$ is a
 121 positive wavenumber, $f \in L^2(\Omega)$ represents a harmonic source, i denotes the
 122 imaginary unit and the scalar diffusion coefficient A is a piecewise constant
 123 with respect to a quadrilateral background mesh \mathcal{T}_ε with mesh size $O(\varepsilon)$ and
 124 $0 < \varepsilon < 1$. On each quadrilateral, A takes either the value ε^2 or 1 . We define
 125 the Sobolev space $V = \{u \in H^1(\Omega) : u = 0 \text{ on } \Gamma_D\}$ and the k -weighted norm

$$\|u\|_V := \|u\|_{1,A,k} := \sqrt{k^2 \|u\|^2 + \|A^{1/2} \nabla u\|^2},$$

126 where $\|\cdot\|$ denotes the L^2 -norm over Ω . We write the boundary value problem
 127 eq. (1) in a variational form and find a solution $u \in V$ such that for all $v \in V$,

$$\int_{\Omega} A \nabla u \cdot \nabla \bar{v} \, dx - ik \int_{\Gamma} u \bar{v} \, ds - \int_{\Omega} k^2 u \bar{v} \, dx = \int_{\Omega} f \bar{v} \, dx, \quad \forall v \in V, \quad (2)$$

128 where ds represents the element of arc length along boundary Γ and $\bar{\cdot}$ is
 129 the complex conjugation. To simplify the notations, the sesquilinear form
 130 $\mathcal{B} : V \times V \rightarrow \mathbb{C}$ satisfies

$$\mathcal{B}(u, v) := (A \nabla u, \nabla v) - ik(u, v)_{\Gamma} - k^2(u, v), \quad (3)$$

131 where $(u, v) = \int_{\Omega} u \cdot \bar{v} \, dx$ and $(u, v)_{\Gamma} = \int_{\Gamma} u \cdot \bar{v} \, ds$. Then we rewrite eq. (2)
 132 in the following

$$\mathcal{B}(u, v) = (f, v). \quad (4)$$

133 The well-posedness of the weak form eq. (4) can be found in [31] and for all
 134 $u, v \in V$ that satisfy the following inf-sup condition is as follows

$$\inf_{u \in V} \sup_{v \in V} \frac{\operatorname{Re} \mathcal{B}(u, v)}{\|u\|_{1,A,k} \|v\|_{1,A,k}} \geq \gamma > 0.$$

Let \mathcal{T}_H be a standard quadrilateralization of the domain Ω with the mesh size H , where we call \mathcal{T}_H coarse grid, $H > 0$ being the coarse grid size. We refer to this partition as coarse grids, and the produced elements as the coarse elements. In each coarse element $K \in \mathcal{T}_H$, K is further partitioned into a union of connected fine grid blocks. We denote the fine-grid partition as \mathcal{T}_h with $h > 0$ being the fine grid size. For each $K_j \in \mathcal{T}_H$ with $1 \leq j \leq N$, N is the number of the coarse grid elements. As is shown in fig. 1 we define an oversampled domain $K_j^m (m \geq 1)$ in the following

$$K_j^m := \text{int} \left\{ \bigcup_{K \in \mathcal{T}_H} \left\{ \overline{K_j^{m-1}} \cap \overline{K} \neq \emptyset \right\} \cup \overline{K_j^{m-1}} \right\},$$

135 where $\text{int}(S)$ and \overline{S} represent the interior and the closure of a set S , and the
initial value $K_j^0 = K_j$ for each element.

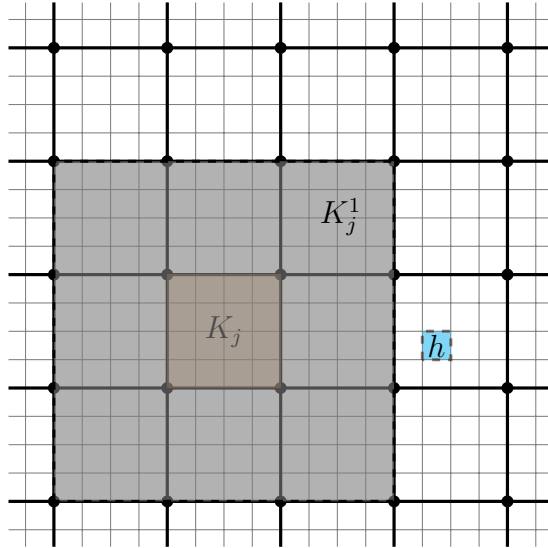


Figure 1: An illustration of the two-scale mesh, a fine element h , a coarse element K_j and its oversampling coarse element K_j^m with the oversampling layer $m = 1$.

136

137 3. The construction of the CEM-GMsFEM basis function

138 In this section, We now present our CEM-GMsFEM to efficiently solve
139 eq. (1). The main process is as the following: we first construct auxiliary

140 basis functions by solving an eigenvalue problem in an coarse element K_j ,
 141 then move on the auxiliary basis functions to the multiscale basis functions
 142 throughout oversampling areas by utilizing the idea of constrained energy
 143 minimization , finally the computational method will also been given and we
 144 solve Helmholtz problems in the newly obtained multiscale basis functions
 145 spaces.

146 Let $V(K_j)$ be the snapshot space on each coarse grid block K_j , and we
 147 use the method of the spectral problem to solve an eigenvalue problem on
 148 K_j : find eigenvalues $\lambda_j^i \in \mathbb{R}$ and basis functions $\phi_j^i \in H^1(K_j)$ such that for
 149 all $v \in V(K_j)$,

$$a_j(\phi_j^i, v) = \lambda_j^i s_j(\phi_j^i, v), \quad \forall v \in H^1(K_j), \quad (5)$$

where

$$a_j(\phi_j^i, v) = \int_{K_j} A \nabla \phi_j^i \cdot \nabla \bar{v} \, dx,$$

$$s_j(\phi_j^i, v) = \int_{K_j} \tilde{A}(x) \phi_j^i \bar{v} \, dx, \quad \tilde{A}(x) := \sum_{k=1}^{N_v} A \nabla \eta_{j,k}^i \cdot \nabla \eta_{j,k}^i,$$

where, N_v is the number of vertices contained in an element, to be specific,
 $N_v = 4$ for a quadrilateral mesh and $\{\eta_{j,1}^i, \eta_{j,2}^i, \dots, \eta_{j,N_v}^i\}$ is the set of La-
 grange basis functions on the coarse element $K_j \in \mathcal{T}_H$. For the function $\tilde{A}(x)$,
 there is a non-negative constant c_* such that

$$c_*^{-1} H^{-2} \min(1, \varepsilon^2) \leq \tilde{A}(x) \leq c_* H^{-2} \max(1, \varepsilon^2).$$

Let the eigenvalues λ_j^i in the ascending order:

$$0 = \lambda_j^0 < \lambda_j^1 \leq \lambda_j^2 \leq \dots \leq \lambda_j^{l_j+1} \leq \dots,$$

and we use the first l_j eigenvalue functions corresponding to the eigen-
 values to construct the local auxiliary space $V_{\text{aux}}^j = \{\phi_j^1, \phi_j^2, \dots, \phi_j^{l_j}\}$. The
 global auxiliary space V_{aux} is the sum of these local auxiliary spaces, namely
 $V_{\text{aux}} = \bigoplus_{j=1}^N V_{\text{aux}}^j$, which will be used to construct multiscale basis functions.
 The next we give the definition of the so called ϕ_j^i -orthogonal, for a given a
 function $\phi_j^i \in V_{\text{aux}}$, $\psi \in V$, and we define

$$s(\phi_j^i, \psi) = 1, \quad s(\phi_{j'}^{i'}, \psi) = 0 \text{ if } j' \neq j \text{ or } i' \neq i.$$

Based on the ϕ_j^i -orthogonal, we can obtain that for any $v \in V$

$$s(\phi_j^i, v) = \sum_{j=1}^N s_j(\phi_j^i, v).$$

The orthogonal projection π_j from $V(K_j)$ onto V_{aux}^j is

$$\pi_j(v) := \sum_{i=1}^{l_j} \frac{s(\phi_j^i, v)}{s(\phi_j^i, \phi_j^i)} \phi_j^i, \quad \forall v \in V(K_j),$$

150 and the global projection is $\pi := \sum_{j=1}^N \pi_j$ from L^2 to V_{aux} .¹ We can immedi-
 151 ately derive the following lemma 3.1, which shows an important property of
 152 the global projection π .

153 **Lemma 3.1.** *In each $K_j \in \mathcal{T}_H$, for all $v \in H^1(K_j)$,*

$$\|v - \pi_j v\|_{s(K_j)}^2 \leq \frac{\|v\|_{a(K_j)}^2}{\lambda_{l_j+1}^j} \leq \Lambda^{-1} \|v\|_{a(K_j)}^2. \quad (6)$$

154 where $\Lambda = \max_{1 \leq j \leq N} \lambda_j^{l_j+1}$, and

$$\|\pi_j v\|_{s(K_j)}^2 = \|v\|_{s(K_j)}^2 - \|v - \pi_j v\|_{s(K_j)}^2 \leq \|v\|_{s(K_j)}^2. \quad (7)$$

155 3.1. Multiscale basis functions

156 In order to deal with the lack of hermitivity of the \mathcal{B} , we need to define
 157 two bounded operators $T_m = \sum_{K_j \in \mathcal{T}_H} T_{j,m}$ and $T_m^* = \sum_{K_j \in \mathcal{T}_H} T_{j,m}^*$ both from
 158 $L^2(\Omega)$ to $H^1(\Omega)$ to construct the test space and trial space of the following
 159 variational problems. For each coarse element $K_j \in \mathcal{T}_H$ and its oversampling
 160 domain $K_j^m \subset \Omega$ by enlarging K_j for m coarse grid layers, we define the
 161 multiscale basis function $T_{j,m} \psi_{j,m}^i \in V_0(K_j^m)$, find $T_{j,m} \psi_{j,m}^i \in V_0(K_j^m)$ such
 162 that

$$\mathcal{B}(T_{j,m} \psi_{j,m}^i, v) + s(\pi T_{j,m} \psi_{j,m}^i, \pi v) = s(\pi_j \psi_{j,m}^i, \pi v), \quad \forall v \in V_0(K_j^m), \quad (8)$$

¹We use a zero-extension here, which extends each V_{aux}^j into $L^2(\Omega)$.

where $V_0(K_j^m)$ is the subspace of $V(K_j^m)$ with zero trace on ∂K_j^m and $V(K_j^m)$ is the restriction of V in K_j^m . Now, our multiscale finite element space V_{ms} can be defined by solving an variational problem eq. (8)

$$V_{\text{ms}} = \text{span}\{T_{j,m}\psi_{j,m}^i \mid 1 \leq i \leq l_j, 1 \leq j \leq N\}.$$

163 The global multiscale basis function $T_j\psi_j^i \in V$ is defined in a similar way,

$$\mathcal{B}(T_j\psi_j^i, v) + s(\pi T_j\psi_j^i, \pi v) = s(\pi_j\psi_j^i, \pi v), \quad \forall v \in V(K_j), \quad (9)$$

and $T = \sum_{K_j \in \mathcal{T}_H} T_j$. Thereby, the global multiscale finite element space V_{glo} is defined by

$$V_{\text{glo}} = \text{span}\{T_j\psi_j^i \mid 1 \leq i \leq l_j, 1 \leq j \leq N\}.$$

164 Similarly, for the local operator $T_{j,m}^*$ from $L^2(K_j^m)$ to $H^1(K_j^m)$,

$$\mathcal{B}(v, T_{j,m}^*\psi_{j,m}^i) + s(\pi v, \pi T_{j,m}^*\psi_{j,m}^i) = s(\pi v, \pi_j\psi_{j,m}^i), \quad \forall v \in V_0(K_j^m), \quad (10)$$

165 where $T_{j,m}^*(v) = \overline{T_{j,m}(\bar{v})}$.

166 **Remark.** Due to the operator \mathcal{B} is in the complex domain, there is no min-
167 imum solutions of the minimization problem listed in [23].

Now, another multiscale finite element space V_{ms}^* can be defined by solving the above variational problem 10

$$V_{\text{ms}}^* = \text{span}\{T_{j,m}^*\psi_{j,m}^i \mid 1 \leq i \leq l_j, 1 \leq j \leq N\}.$$

168 The global multiscale basis function $T_j^*\psi_j^i \in V$ is defined in a similar way,

$$\mathcal{B}(v, T_j^*\psi_j^i) + s(\pi v, \pi T_j^*\psi_j^i) = s(\pi v, \pi_j\psi_j^i), \quad \forall v \in V(K_j), \quad (11)$$

where $T^* = \sum_{K_j \in \mathcal{T}_H} T_j^*$. Thereby, another global multiscale finite element space V_{glo}^* is defined by

$$V_{\text{glo}}^* = \text{span}\{T_j^*\psi_j^i \mid 1 \leq i \leq l_j, 1 \leq j \leq N\}.$$

169 The existence of the above two variational problems will be shown in the
170 analysis part. In the following, we use V_{ms} and V_{ms}^* as the new test space and
171 trial space of Petrov-Galerkin method to find the approximated solution of
172 eq. (4): Find $u_{\text{ms}} \in V_{\text{ms}}$ such that

$$\mathcal{B}(u_{\text{ms}}, v) = (f, v), \quad \forall v \in V_{\text{ms}}^*. \quad (12)$$

173 For further analysis, we need to clarify an important orthogonality property
174 of the global multiscale finite element space V_{glo} and V_{glo}^* .

Lemma 3.2. *The space V is decomposed as*

$$V = \tilde{V} \oplus V_{\text{glo}}^*,$$

175 where $\tilde{V} = \{v \in V \mid \pi(v) = 0\}$ and $W = \{v \in V \mid \mathcal{B}(v, w) = 0, \forall w \in V_{\text{glo}}^*\}$,
176 then $\tilde{V} = W$.

177 *Proof.* By using the fact in eq. (11), it is easy to see $\tilde{V} \subset W$. For another
178 direction, $\forall v_0 \in W$, we have $\mathcal{B}(v_0, w) = 0$. Then we can obtain $s(\pi v_0, \pi w) =$
179 $s(\pi v_0, \pi \psi_j^i)$. Due to the arbitrary $w \in V_{\text{glo}}^*$, we can get that $\pi v_0 = 0$ and
180 $W \subset \tilde{V}$. \square

Lemma 3.3. *The space V is also decomposed as*

$$V = \tilde{V} \oplus V_{\text{glo}},$$

181 where $\tilde{V} = \{v \in V \mid \pi(v) = 0\}$ and $\tilde{W} = \{v \in V \mid \mathcal{B}(w, v) = 0, \forall w \in V_{\text{glo}}\}$,
182 then $\tilde{V} = \tilde{W}$.

183 *Proof.* By using the fact in eq. (9), it is easy to see $\tilde{V} \subset \tilde{W}$. For another
184 direction, $\forall v_0 \in \tilde{W}$, we have $\mathcal{B}(w, v_0) = 0$. Then we can obtain $s(\pi w, \pi v_0) =$
185 $s(\pi v_0, \pi \psi_j^i)$. Due to the arbitrary $w \in V_{\text{glo}}$, we can get that $\pi v_0 = 0$ and
186 $\tilde{W} \subset \tilde{V}$. \square

187 **Remark.** *The above two lemmas show a relationship of “orthogonality” be-*
188 *tween \tilde{V} and its complementary space $V_{\text{glo}}, V_{\text{glo}}^*$ concerning the bilinear form*
189 *$\mathcal{B}(\cdot, \cdot)$. However, we must be cautious in using the term “orthogonal” since*
190 *$\mathcal{B}(\cdot, \cdot)$ cannot define an inner product on V .*

191 4. Analysis

192 In this section, we give the stability and convergence of CEM-GMsFEM
193 by using the global multiscale basis functions. We firstly prove that the
194 sesquilinear form of a is coercive, continuous and bounded. Then we show the
195 exponential decay property of the multiscale basis functions. In particular,
196 we will show that the the global basis function and the corresponding local
197 basis function are the same the if the oversampling region is sufficiently large.
198 Finally, we prove the convergence of the multiscale solution in our main result
199 theorem 4.9. Here, the approximated solution $u_{\text{glo}} \in V_{\text{glo}}$ obtained in the
200 global multiscale space V_{glo} is defined by

$$\mathcal{B}(u_{\text{glo}}, v) = (f, v), \quad \forall v \in V_{\text{glo}}^*. \quad (13)$$

Lemma 4.1. *If the mesh size H , the wave number k , and diffusion parameter ε satisfies the resolution condition such that*

$$\sqrt{2c_*}kH\varepsilon^{-1} \leq 1,$$

201 *the sesquilinear form defined in eq. (3) is continuous on V , that is*

$$|\mathcal{B}(u, v)| \leq c\|u\|_{1,A,k}\|v\|_{1,A,k} \quad \forall u, v \in V, \quad (14)$$

202 *where c is independent of k , and the sesquilinear form is coercive on \tilde{V} defined*
 203 *in lemma 3.2,*

$$\epsilon_0\|v\|_a^2 \leq \operatorname{Re} \mathcal{B}(v, v), \quad \forall v \in \tilde{V}, \quad (15)$$

204 *where Re and Im represents the real and imaginary parts of a complex num-*
 205 *ber, respectively.*

Proof. Rewrite the definition of $\mathcal{B}(u, v)$ in eq. (3), we have

$$\mathcal{B}(u, v) = b_1 + b_2 + b_\Gamma,$$

206 where

$$b_1(u, v) := \int_{\Omega} (A\nabla u \cdot \nabla \bar{v} + k^2 u \bar{v}) \, dx,$$

$$b_2(u, v) := -2k^2 \int_{\Omega} u \bar{v} \, dx, \quad b_\Gamma := -ik \int_{\Gamma} u \bar{v} \, dx.$$

By using the Cauchy–Schwartz inequality we obtain

$$|b_1(u, v)| \leq \|u\|_{1,A,k}\|v\|_{1,A,k},$$

$$|b_2(u, v)| \leq 2\|u\|_{1j,A,k}\|v\|_{1,A,k},$$

and the trace inequalities from [32],

$$|b_\Gamma(u, v)| \leq C_\Gamma\|u\|_{1,A,k}\|v\|_{1,A,k},$$

where C_Γ is independent of k . By using the interpolation properties of the operator π in lemma 3.1 and assumption about the resolution condition

$$\operatorname{Re} \mathcal{B}(v, v) = \|v\|_a^2 - k^2\|v\|^2 \geq (\Lambda - c_*k^2H^2\varepsilon^{-2})\|v\|_s^2 \geq \epsilon_0\|v\|_a^2,$$

207 where the eigenvalue Λ is chosen such that $\Lambda \geq \frac{1}{2} + \epsilon_0$ and ϵ_0 is a small
 208 positive value. \square

209 The following lemma gives the well-posedness of the global multiscale
 210 problem eq. (13) by proving the inf-sup condition.

211 **Lemma 4.2.** *The bilinear form \mathcal{B} satisfies the following inf-sup condition:*
 212 *there exists a constant $\gamma > 0$ depends on k such that*

$$\inf_{u_{\text{glo}} \in V_{\text{glo}}} \sup_{u_{\text{glo}}^* \in V_{\text{glo}}^*} \frac{\text{Re } \mathcal{B}(u_{\text{glo}}, u_{\text{glo}}^*)}{\|u_{\text{glo}}\|_{1,A,k} \|u_{\text{glo}}^*\|_{1,A,k}} \geq \gamma > 0.$$

213 Based on the previous decomposition of the space V , the Fortin trick [33]
 214 suggests that we only need to check

$$\inf_{v_1 \in \tilde{V}} \sup_{v_2 \in \tilde{V}} \frac{\text{Re } \mathcal{B}(v_1, v_2)}{\|v_1\|_{1,A,k} \|v_2\|_{1,A,k}} \geq \gamma > 0.$$

Proof. For any $v_1 \in \tilde{V}$, we apply the inf-sup condition of the $\mathcal{B}(u, v)$ in $V \times V$,
 for any $v_2 \in V$, there exists a $\phi \in V$ and $\|\phi\|_{1,A,k} = 1$. such that

$$\text{Re } \mathcal{B}(v_1, \phi) \geq \gamma \|v_1\|_{1,A,k}.$$

Then we can define $v_2 = \phi - T^* \phi \in \tilde{V}$, and $\mathcal{B}(v_1, v_2) = \mathcal{B}(v_1, \phi) - \mathcal{B}(v_1, T^* \phi) =$
 $\mathcal{B}(v_1, \phi)$, where the last equality comes from the fact that $\mathcal{B}(v_1, T^* \phi) = 0$.
 Since $\mathcal{B}(v_1, T^* \phi) = \mathcal{B}(T\bar{\phi}, \bar{v}_1) = 0$ where $T\bar{\phi} \in V_{\text{glo}}$ and $\bar{v}_1 \in \tilde{V}$, by using
 of the orthogonality in lemma 3.3, especially, we can obtain $\mathcal{B}(T\bar{\phi}, \bar{v}_1) = 0$.
 Finally we can obtain the desired inequality that

$$\text{Re } \mathcal{B}(v_1, v_2) = \text{Re } \mathcal{B}(v_1, \phi) \geq \gamma \|v_1\|_{1,A,k} \geq \gamma \|v_1\|_{1,A,k} \|v_2\|_{1,A,k},$$

215 where the last inequality comes from that $\|v_2\|_{1,A,k} \leq \|\phi\|_{1,A,k} + \|T^* \phi\|_{1,A,k} \leq$
 216 $(1 + C)\|\phi\|_{1,A,k}$ due to the bounded operator T^* . \square

217 After obtaining the well-posedness of the global problem, an error esti-
 218 mate of the global solution can be derived in lemma 4.3 .

Lemma 4.3. *By using the resolution condition in lemma 4.1, let u_{glo} be the
 solution of eq. (13) and u be the real solution of the problem eq. (4). Then*

$$\|u_{\text{glo}} - u\|_a \leq \frac{1}{\epsilon_0 \sqrt{\Lambda}} \|f\|_{s^{-1}},$$

where $\Lambda = \max_{1 \leq j \leq N} \lambda_{l_j+1}^j$, and

$$\|f\|_{s^{-1}} := \sup_{v \in L^2(\Omega), v \neq 0} \frac{\int_{\Omega} f v \, dx}{\|v\|_s}.$$

Proof. By direct computation in eq. (13) and eq. (4), we obtain the Galerkin orthogonality that for any $v \in V_{\text{glo}}^*$

$$\mathcal{B}(u - u_{\text{glo}}, v) = 0.$$

219 In lemma 3.2, we have $\mathcal{B}(u - u_{\text{glo}}, v) = 0$, thus $u - u_{\text{glo}} \in \tilde{V}$ and $\pi(u - u_{\text{glo}}) =$
220 0. By using coercivity of \mathcal{B} on \tilde{V} and variational form in eq. (4), we have

$$\begin{aligned} \epsilon_0 \|u - u_{\text{glo}}\|_a^2 &\leq \text{Re } \mathcal{B}(u - u_{\text{glo}}, u - u_{\text{glo}}) \\ &\leq |\mathcal{B}(u, u - u_{\text{glo}})| \\ &= |(f, u - u_{\text{glo}})| \\ &\leq \|f\|_{s-1} \|u - u_{\text{glo}}\|_s = \|f\|_{s-1} \|u - u_{\text{glo}} - \pi(u - u_{\text{glo}})\|_s \\ &\leq \frac{1}{\sqrt{\Lambda}} \|f\|_{s-1} \|u - u_{\text{glo}}\|_a, \end{aligned}$$

221 where the last inequality comes from eq. (5) directly. \square

222 The following lemma 4.4 will show the multiscale basis functions have the
223 exponentially decaying property. Before we give the detailed proof, we need
224 to define the cutoff functions with respect to these oversampling domains in
225 the following.

For the cutoff functions, in each K_j , let V_H be the Lagrange basis function space of \mathcal{T}_H , we define $\eta_j^{n,m} \in V_H, m > n$ such that $0 \leq \eta_j^{n,m} \leq 1$ and

$$\begin{aligned} \eta_j^{n,m} &= 0, \quad \text{in } K_{j,n}, \\ \eta_j^{n,m} &= 1, \quad \text{in } \Omega \setminus K_{j,m}, \\ 0 \leq \eta_j^{n,m} &\leq 1, \quad \text{in } K_{j,m} \setminus K_{j,n}. \end{aligned}$$

Lemma 4.4. *There exists a constant $0 < \beta < 1$, independent of H, m and k such that for any $t_j \in V_H$,*

$$\|T_j t_j\|_{a(\Omega \setminus K_{j,m})}^2 + \|\pi T_j t_j\|_{s(\Omega \setminus K_{j,m})}^2 \leq \beta^m (\|T_j t_j\|_a^2 + \|\pi T_j t_j\|_s^2),$$

226 where $\beta = \frac{C}{1+C}$.

Proof. Let $t_j \in V_H$, and choose $w = \eta_j^{m-1,m} T_j t_j$ with support only outside $K_{j,m-1}$, therefore we obtain $\mathcal{B}(T_j t_j, w) + s(\pi T_j t_j, \pi w) = 0$. By recalling the

definition of the operator \mathcal{B} we have

$$\begin{aligned} & \int_{\Omega} A \nabla T_j t_j \cdot \nabla \overline{(\eta_j^{m-1,m} T_j t_j)} dx + \int_{\Omega} \tilde{A} \pi T_j t_j \cdot \pi \overline{(\eta_j^{m-1,m} T_j t_j)} dx \\ &= ik \int_{\Gamma} T_j t_j \cdot \overline{(\eta_j^{m-1,m} T_j t_j)} ds + k^2 \int_{\Omega} T_j t_j \cdot \overline{(\eta_j^{m-1,m} T_j t_j)} dx. \end{aligned}$$

By using the properties of the cutoff functions to observe that $1 - \eta_j^{m-1,m} = 0$ in $\Omega \setminus K_{j,m}$ and $1 - \eta_j^{m-1,m} = 1$ in $K_{j,m-1}$, we can obtain

$$\begin{aligned} & \|T_j t_j\|_{a(\Omega \setminus K_{j,m})}^2 + \|\pi T_j t_j\|_{s(\Omega \setminus K_{j,m})}^2 \\ &= - \int_{K_{j,m} \setminus K_{j,m-1}} \eta_j^{m-1,m} A \nabla T_j t_j \cdot \nabla \overline{T_j t_j} dx - \int_{K_{j,m} \setminus K_{j,m-1}} \overline{T_j t_j} A \nabla T_j t_j \cdot \nabla \eta_j^{m-1,m} dx \\ & \quad - \int_{K_{j,m} \setminus K_{j,m-1}} \tilde{A} \pi T_j t_j \cdot \pi \overline{(\eta_j^{m-1,m} T_j t_j)} dx \\ & \quad + ik \int_{\Gamma} T_j t_j \cdot \overline{(\eta_j^{m-1,m} T_j t_j)} ds + k^2 \int_{\Omega} T_j t_j \cdot \overline{(\eta_j^{m-1,m} T_j t_j)} dx \\ &= - \operatorname{Re} \int_{K_{j,m} \setminus K_{j,m-1}} \eta_j^{m-1,m} A \nabla T_j t_j \cdot \nabla \overline{T_j t_j} dx - \operatorname{Re} \int_{K_{j,m} \setminus K_{j,m-1}} \overline{T_j t_j} A \nabla T_j t_j \cdot \nabla \eta_j^{m-1,m} dx \\ & \quad - \operatorname{Re} \int_{K_{j,m} \setminus K_{j,m-1}} \tilde{A} \pi T_j t_j \cdot \pi \overline{(\eta_j^{m-1,m} T_j t_j)} dx \\ & \quad + \operatorname{Re} \left(ik \int_{\Gamma} T_j t_j \cdot \overline{(\eta_j^{m-1,m} T_j t_j)} ds \right) + \operatorname{Re} \left(k^2 \int_{\Omega} T_j t_j \cdot \overline{(\eta_j^{m-1,m} T_j t_j)} dx \right) \\ &\leq \left| \operatorname{Re} \int_{K_{j,m} \setminus K_{j,m-1}} \eta_j^{m-1,m} A \nabla T_j t_j \cdot \nabla \overline{T_j t_j} dx \right| + \left| \operatorname{Re} \int_{K_{j,m} \setminus K_{j,m-1}} \overline{T_j t_j} A \nabla T_j t_j \cdot \nabla \eta_j^{m-1,m} dx \right| \\ & \quad + \left| \operatorname{Re} \int_{K_{j,m} \setminus K_{j,m-1}} \tilde{A} \pi T_j t_j \cdot \pi \overline{(\eta_j^{m-1,m} T_j t_j)} dx \right| \\ & \quad + \left| \operatorname{Re} \left(ik \int_{\Gamma} T_j t_j \cdot \overline{(\eta_j^{m-1,m} T_j t_j)} ds \right) \right| + \left| \operatorname{Re} \left(k^2 \int_{\Omega} T_j t_j \cdot \overline{(\eta_j^{m-1,m} T_j t_j)} dx \right) \right| \\ &= \sum_{i=1}^5 I_i. \end{aligned}$$

227 For I_4 , due to the property of the cutoff function, we can obtain

$$I_4 = \left| \operatorname{Re} \left(ik \int_{\Gamma} T_j t_j \cdot \overline{(\eta_j^{m-1,m} T_j t_j)} ds \right) \right| = 0.$$

228 Combining with the properties of $\eta_j^{m-1,m}$ and the resolution condition gives

$$I_5 \leq \left| k^2 \int_{\Omega \setminus K_{j,m-1}} T_j t_j \cdot \overline{T_j t_j} \, dx \right| \leq \frac{1}{2} (\|T_j t_j\|_{s(\Omega \setminus K_{j,m})}^2 + \|T_j t_j\|_{s(K_{j,m} \setminus K_{j,m-1})}^2).$$

Also, eq. (6) provides an estimate for $\|T_j t_j\|_{s(K_{j,m} \setminus K_{j,m-1})}$ and $\|T_j t_j\|_{s(\Omega \setminus K_{j,m})}$,

$$\begin{aligned} \|T_j t_j\|_{s(K_{j,m} \setminus K_{j,m-1})}^2 &\leq \|T_j t_j - \pi T_j t_j\|_{s(K_{j,m} \setminus K_{j,m-1})}^2 + \|\pi T_j t_j\|_{s(K_{j,m} \setminus K_{j,m-1})}^2 \\ &\leq \frac{1}{\Lambda} \|T_j t_j\|_{a(K_{j,m} \setminus K_{j,m-1})}^2 + \|\pi T_j t_j\|_{s(K_{j,m} \setminus K_{j,m-1})}^2, \end{aligned}$$

and

$$\begin{aligned} \|T_j t_j\|_{s(\Omega \setminus K_{j,m})}^2 &\leq \|T_j t_j - \pi T_j t_j\|_{s(\Omega \setminus K_{j,m})}^2 + \|\pi T_j t_j\|_{s(\Omega \setminus K_{j,m})}^2 \\ &\leq \frac{1}{\Lambda} \|T_j t_j\|_{a(\Omega \setminus K_{j,m})}^2 + \|\pi T_j t_j\|_{s(\Omega \setminus K_{j,m})}^2. \end{aligned}$$

By the definition of \tilde{A} , it is easy to show

$$A(x) \nabla \eta_j^{m-1,m} \cdot \nabla \eta_j^{m-1,m} \leq \tilde{A}(x),$$

and using the properties of $\eta_j^{m-1,m}$, the estimates of I_2 follows

$$I_2 \leq \|T_j t_j\|_{a(K_{j,m} \setminus K_{j,m-1})} \|T_j t_j\|_{s(K_{j,m} \setminus K_{j,m-1})}.$$

For the term I_3 , using the Cauchy-Schwarz inequality, we have

$$\begin{aligned} I_3 &\leq \|\pi T_j t_j\|_{s(K_{j,m} \setminus K_{j,m-1})} \|\pi(\eta_j^{m-1,m} T_j t_j)\|_{s(K_{j,m} \setminus K_{j,m-1})} \\ &\leq \|\pi T_j t_j\|_{s(K_{j,m} \setminus K_{j,m-1})} \|\eta_j^{m-1,m} T_j t_j\|_{s(K_{j,m} \setminus K_{j,m-1})} \\ &\leq \|\pi T_j t_j\|_{s(K_{j,m} \setminus K_{j,m-1})} \|T_j t_j\|_{s(K_{j,m} \setminus K_{j,m-1})}. \end{aligned}$$

For the last term I_1 , Due to the definition of $\eta_j^{m-1,m}$, we can derive

$$I_1 \leq \|T_j t_j\|_{a(K_{j,m} \setminus K_{j,m-1})}^2.$$

Combining all above estimates of I_1 to I_5 together, we obtain

$$\begin{aligned} &\left(1 - \frac{1}{2\Lambda}\right) \|T_j t_j\|_{a(\Omega \setminus K_{j,m})}^2 + \frac{1}{2} \|\pi T_j t_j\|_{s(\Omega \setminus K_{j,m})}^2 \\ &\leq C (\|T_j t_j\|_{a(K_{j,m} \setminus K_{j,m-1})}^2 + \|\pi T_j t_j\|_{s(K_{j,m} \setminus K_{j,m-1})}^2), \end{aligned}$$

also, we need to choose $\Lambda > \frac{1}{2}$ to future derive

$$\begin{aligned} & \|T_j t_j\|_{a(\Omega \setminus K_{j,m})}^2 + \|\pi T_j t_j\|_{s(\Omega \setminus K_{j,m})}^2 \\ & \leq C(\Lambda) (\|T_j t_j\|_{a(K_{j,m} \setminus K_{j,m-1})}^2 + \|\pi T_j t_j\|_{s(K_{j,m} \setminus K_{j,m-1})}^2). \end{aligned}$$

Because of

$$\begin{aligned} & \|T_j t_j\|_{a(\Omega \setminus K_{j,m})}^2 + \|T_j t_j\|_{a(K_{j,m} \setminus K_{j,m-1})}^2 = \|T_j t_j\|_{a(K_{j,m-1})}^2, \\ & \|\pi T_j t_j\|_{s(\Omega \setminus K_{j,m})}^2 + \|\pi T_j t_j\|_{s(K_{j,m} \setminus K_{j,m-1})}^2 = \|\pi T_j t_j\|_{s(K_{j,m-1})}^2, \end{aligned}$$

then

$$\begin{aligned} & \|T_j t_j\|_{a(\Omega \setminus K_{j,m})}^2 + \|\pi T_j t_j\|_{s(\Omega \setminus K_{j,m})}^2 \\ & \leq \frac{C(\Lambda)}{1 + C(\Lambda)} (\|T_j t_j\|_{a(\Omega \setminus K_{j,m-1})}^2 + \|\pi T_j t_j\|_{s(\Omega \setminus K_{j,m-1})}^2). \end{aligned}$$

Let $\beta = \frac{C(\Lambda)}{1 + C(\Lambda)} < 1$, and after repeat the above the inequality

$$\|T_j t_j\|_{a(\Omega \setminus K_{j,m})}^2 + \|\pi T_j t_j\|_{s(\Omega \setminus K_{j,m})}^2 \leq \beta^m (\|T_j t_j\|_a^2 + \|\pi T_j t_j\|_s^2).$$

229

□

Lemma 4.5. *Keep the notations same as lemma 4.4, then for $t_j \in V_H$, there exists a constant $C(\Lambda)$ such that*

$$\|(T_j - T_{j,m})t_j\|_a^2 + \|\pi(T_j - T_{j,m})t_j\|_s^2 \leq C(\Lambda)\beta^{m-1}(\|T_j t_j\|_a^2 + \|\pi T_j t_j\|_s^2).$$

230 *Proof.* By using the previous definition of the operators T_j and $T_{j,m}$, subtract
231 each other we can obtain for $w = (1 - \eta_j^{m-1,m})T_j t_j - T_{j,m}t_j \in V_{j,m}$,

$$\mathcal{B}(T_j t_j - T_{j,m}t_j, w) + s(\pi(T_j t_j - T_{j,m}t_j), \pi w) = 0.$$

232 After reformulating the above equation,

$$\begin{aligned} & \mathcal{B}(T_j t_j - T_{j,m}t_j, T_j t_j - T_{j,m}t_j) + s(\pi(T_j t_j - T_{j,m}t_j), \pi(T_j t_j - T_{j,m}t_j)) \\ & = \mathcal{B}(T_j t_j - T_{j,m}t_j, \eta_j^{m-1,m}T_j t_j) + s(\pi(T_j t_j - T_{j,m}t_j), \pi(\eta_j^{m-1,m}T_j t_j)). \end{aligned}$$

233 Recalling the definition of the operator \mathcal{B} , we obtain

$$\begin{aligned}
& \|(T_j - T_{j,m})t_j\|_a^2 + \|\pi(T_j - T_{j,m})t_j\|_s^2 \\
&= a(T_j t_j - T_{j,m} t_j, \eta_j^{m-1,m} T_j t_j) + s(\pi(T_j t_j - T_{j,m} t_j), \pi(\eta_j^{m-1,m} T_j t_j)) \\
&\quad + ik(T_j t_j - T_{j,m} t_j, w)_\Gamma + k^2(T_j t_j - T_{j,m} t_j, w) \\
&= \operatorname{Re}(a(T_j t_j - T_{j,m} t_j, \eta_j^{m-1,m} T_j t_j)) + \operatorname{Re}(s(\pi(T_j t_j - T_{j,m} t_j), \pi(\eta_j^{m-1,m} T_j t_j))) \\
&\quad + \operatorname{Re}(ik(T_j t_j - T_{j,m} t_j, w)_\Gamma) + \operatorname{Re}(k^2(T_j t_j - T_{j,m} t_j, w)) \\
&\leq |\operatorname{Re}(a(T_j t_j - T_{j,m} t_j, \eta_j^{m-1,m} T_j t_j))| + |\operatorname{Re}(s(\pi(T_j t_j - T_{j,m} t_j), \pi(\eta_j^{m-1,m} T_j t_j)))| \\
&\quad + |\operatorname{Re}(ik(T_j t_j - T_{j,m} t_j, w)_\Gamma)| + |\operatorname{Re}(k^2(T_j t_j - T_{j,m} t_j, w))| \\
&= \sum_{i=1}^4 I_i.
\end{aligned}$$

234 For I_3 , we use the trace inequality in [34] to obtain

$$\begin{aligned}
I_3 &\leq |\operatorname{Re}(ik(T_j t_j - T_{j,m} t_j, w)_\Gamma)| \\
&\leq |k(T_j t_j - T_{j,m} t_j, \eta_j^{m-1,m} T_j t_j)_\Gamma| \\
&\leq \|(T_j - T_{j,m})t_j\|_{1,A,k} \|\eta_j^{m-1,m} T_j t_j\|_{1,A,k} \\
&\leq (\|(T_j - T_{j,m})t_j\|_a^2 + k^2\|(T_j - T_{j,m})t_j\|_s^2)^{1/2} (\|\eta_j^{m-1,m} T_j t_j\|_a^2 + k^2\|\eta_j^{m-1,m} T_j t_j\|_s^2)^{1/2}.
\end{aligned}$$

235 By using resolution condition

$$\begin{aligned}
k^2\|(T_j - T_{j,m})t_j\|_s^2 &\leq c_* k^2 H^2 \varepsilon^{-2} \|(T_j - T_{j,m})t_j\|_s^2 \leq \frac{1}{2} \|(T_j - T_{j,m})t_j\|_s^2, \\
k^2\|\eta_j^{m-1,m} T_j t_j\|_s^2 &\leq c_* k^2 H^2 \varepsilon^{-2} \|T_j t_j\|_{s(\Omega \setminus K_{j,m-1})}^2 \leq \frac{1}{2} \|T_j t_j\|_{s(\Omega \setminus K_{j,m-1})}^2.
\end{aligned}$$

Furthermore,

$$\begin{aligned}
\|(T_j - T_{j,m})t_j\|_s^2 &\leq \|T_j t_j - T_{j,m} t_j - \pi(T_j t_j - T_{j,m} t_j)\|_s^2 + \|\pi((T_j - T_{j,m})t_j)\|_s^2 \\
&\leq \frac{1}{\Lambda} \|(T_j - T_{j,m})t_j\|_a^2 + \|\pi((T_j - T_{j,m})t_j)\|_s^2, \\
\|T_j t_j\|_{s(\Omega \setminus K_{j,m-1})}^2 &\leq \|T_j t_j - \pi T_j t_j\|_{s(\Omega \setminus K_{j,m-1})}^2 + \|\pi T_j t_j\|_{s(\Omega \setminus K_{j,m-1})}^2 \\
&\leq \frac{1}{\Lambda} \|T_j t_j\|_{a(\Omega \setminus K_{j,m-1})}^2 + \|\pi T_j t_j\|_{s(\Omega \setminus K_{j,m-1})}^2.
\end{aligned}$$

Combining with the property of π and the definition of $\eta_j^{m-1,m}$ to obtain

$$\begin{aligned}
\|\eta_j^{m-1,m} T_j t_j\|_a^2 &\leq \|T_j t_j\|_{a(\Omega \setminus K_{j,m-1})}^2 + \|T_j t_j\|_{s(\Omega \setminus K_{j,m-1})}^2 \\
&\leq \left(1 + \frac{1}{\Lambda}\right) \|T_j t_j\|_{a(\Omega \setminus K_{j,m-1})}^2 + \|\pi T_j t_j\|_{s(\Omega \setminus K_{j,m-1})}^2.
\end{aligned}$$

Finally,

$$I_3 \leq C(\Lambda) (\|(T_j - T_{j,m})t_j\|_a^2 + \|(T_j - T_{j,m})t_j\|_s^2)^{1/2} \\ (\|T_j t_j\|_{a(\Omega \setminus K_{j,m-1})}^2 + \|\pi T_j t_j\|_{s(\Omega \setminus K_{j,m-1})}^2)^{1/2}.$$

236 Similarly, we can use the resolution condition for I_4 ,

$$I_4 \leq c_* k^2 H^2 \varepsilon^{-2} (\|(T_j - T_{j,m})t_j\|_s^2 + \|((T_j - T_{j,m})t_j, \eta_j^{m-1,m} T_j t_j)\|_s) \\ \leq \frac{1}{2} \|(T_j - T_{j,m})t_j\|_s^2 + \frac{1}{2} \|((T_j - T_{j,m})t_j, \eta_j^{m-1,m} T_j t_j)\|_s.$$

By using the similar tricks in analysing I_3 ,

$$I_4 \leq \frac{1}{2\Lambda} \|(T_j - T_{j,m})t_j\|_a^2 + \frac{1}{2} \|\pi((T_j - T_{j,m})t_j)\|_s^2 \\ + C(\Lambda) (\|(T_j - T_{j,m})t_j\|_a^2 + \|(T_j - T_{j,m})t_j\|_s^2)^{1/2} \\ (\|T_j t_j\|_{a(\Omega \setminus K_{j,m-1})}^2 + \|\pi T_j t_j\|_{s(\Omega \setminus K_{j,m-1})}^2)^{1/2}.$$

For the remaining terms I_1 and I_2 , we can use Cauchy-Schwarz inequality,

$$I_1 \leq \|(T_j - T_{j,m})t_j\|_a \|\eta_j^{m-1,m} T_j t_j\|_a, I_2 \leq \|\pi((T_j - T_{j,m})t_j)\|_s \|\pi(\eta_j^{m-1,m} T_j t_j)\|_s.$$

We still need to provide a estimate for $\|\pi(\eta_j^{m-1,m} T_j t_j)\|_s$ by using the property of π and the definition of $\eta_j^{m-1,m}$ to obtain

$$\|\pi(\eta_j^{m-1,m} T_j t_j)\|_s \leq \|\eta_j^{m-1,m} T_j t_j\|_s \leq \|T_j t_j\|_{s(\Omega \setminus K_{j,m-1})} \\ \leq \frac{1}{\sqrt{\Lambda}} \|T_j t_j\|_{a(\Omega \setminus K_{j,m-1})} + \|\pi T_j t_j\|_{s(\Omega \setminus K_{j,m-1})}.$$

By combining all above together,

$$\left(1 - \frac{1}{2\Lambda}\right) \|(T_j - T_{j,m})t_j\|_a^2 + \frac{1}{2} \|\pi(T_j - T_{j,m})t_j\|_s^2 \\ \leq C(\Lambda) (\|(T_j - T_{j,m})t_j\|_a^2 + \|\pi(T_j - T_{j,m})t_j\|_s^2)^{1/2} \\ (\|T_j t_j\|_{a(\Omega \setminus K_{j,m-1})}^2 + \|\pi T_j t_j\|_{s(\Omega \setminus K_{j,m-1})}^2)^{1/2} \\ \leq C(\Lambda) \{C_{\text{ol}}(m+1)^d (\|z\|_a^2 + \|\pi z\|_s^2)\}^{1/2} \left\{ \sum_{j=1}^N (\mathcal{B}(z_j, z_j) + s(\pi z_j, \pi z_j)) \right\}^{1/2}.$$

We can choose $\Lambda \geq \frac{1}{2}$ to obtain

$$\begin{aligned} & \|(T_j - T_{j,m})t_j\|_a^2 + \|\pi(T_j - T_{j,m})t_j\|_s^2 \\ & \leq C(\Lambda)(\|(T_j - T_{j,m})t_j\|_a^2 + \|\pi(T_j - T_{j,m})t_j\|_s^2)^{1/2} \\ & \quad (\|T_j t_j\|_{a(\Omega \setminus K_{j,m-1})}^2 + \|\pi T_j t_j\|_{s(\Omega \setminus K_{j,m-1})}^2)^{1/2}. \end{aligned}$$

237 By using the lemma 4.4, we can derive the conclusion. \square

Before we proceed the next proof, we need a assumption of shape regularity for $K_j \in \mathcal{T}_H$ such that there is a bound C_{ol} and $m > 0$,

$$\text{card}\{K \in \mathcal{T}_H : K \subset K_j^m\} \leq C_{ol} m^d.$$

Lemma 4.6. *There exists a constant $0 < \beta < 1$, independent of H, m and k such that for any $t_j \in V_H$*

$$\left\| \sum_{j=1}^N (T_j - T_{j,m})t_j \right\|_a^2 + \left\| \pi \sum_{j=1}^N (T_j - T_{j,m})t_j \right\|_s^2 \leq C^2(\Lambda) C_{ol} \beta^m (m+1)^d \sum_{j=1}^N s(\pi t_j, \pi T t_j).$$

238 *Proof.* To obtain the global estimate, we set $z := \sum_{j=1}^N (T_j - T_{j,m})t_j$ and
 239 $z_j := (T_j - T_{j,m})t_j$. Due to $\text{supp}(\eta_j^{m,m+1} z) \subset \Omega \setminus K_{j,m}$, $\text{supp}(\pi(\eta_j^{m,m+1} z)) \subset$
 240 $\Omega \setminus K_{j,m}$, $\text{supp}(T_{j,m} t_j) \subset \overline{K_{j,m}}$ and $\text{supp}(\pi T_{j,m} t_j) \subset \overline{K_{j,m}}$, By using the
 241 previous definition of the operators T_j and $T_{j,m}$, after subtracting each other
 242 we have

$$\mathcal{B}(z_j, \eta_j^{m,m+1} z) + s(\pi z_j, \pi \eta_j^{m,m+1} z) = 0.$$

243 After reformulating the above equation and using the definition of the oper-
 244 ator \mathcal{B}

$$\begin{aligned} \mathcal{B}(z_j, z) + s(\pi z_j, \pi z) &= \mathcal{B}(z_j, z - \eta_j^{m,m+1} z) + s(\pi z_j, \pi(z - \eta_j^{m,m+1} z)) \\ &= a(z_j, z - \eta_j^{m,m+1} z) + s(\pi z_j, \pi(z - \eta_j^{m,m+1} z)) \quad (16) \\ &\quad - ik(z_j, z - \eta_j^{m,m+1} z)_\Gamma - k^2(z_j, z - \eta_j^{m,m+1} z). \end{aligned}$$

245 For the last four terms of the above, we take the absolute value of them and
 246 use the Trace inequality,

$$\begin{aligned} |ik(z_j, z - \eta_j^{m,m+1} z)_\Gamma| &\leq \|z_j\|_{1,A,k} \|z - \eta_j^{m,m+1} z\|_{1,A,k} \\ &\leq (\|z_j\|_a^2 + k^2 \|z_j\|^2)^{1/2} (\|z - \eta_j^{m,m+1} z\|_a^2 + k^2 \|z - \eta_j^{m,m+1} z\|)^{1/2}. \end{aligned}$$

247 by using resolution condition again,

$$|k^2(z_j, z - \eta_j^{m,m+1}z)| \leq c_* k^2 H^2 \varepsilon^{-2} (\|z_j\|_s \|z - \eta_j^{m,m+1}z\|_s) \leq \frac{1}{2} \|z_j\|_s \|z - \eta_j^{m,m+1}z\|_s.$$

248 Then taking the absolute value of both hand sides of eq. (16)

$$\begin{aligned} & |\mathcal{B}(z_j, z) + s(\pi z_j, \pi z)| \\ & \leq \|z_j\|_a \|z - \eta_j^{m,m+1}z\|_a + \|\pi z_j\|_s \|\pi(z - \eta_j^{m,m+1}z)\|_s + \frac{1}{2} \|z_j\|_s \|z - \eta_j^{m,m+1}z\|_s \\ & \quad + (\|z_j\|_a^2 + k^2 \|z_j\|_s^2)^{1/2} (\|z - \eta_j^{m,m+1}z\|_a^2 + k^2 \|z - \eta_j^{m,m+1}z\|_s^2)^{1/2} \\ & = \sum_{i=1}^4 I_i. \end{aligned}$$

We can similarly use the property of π and the definition of $\eta_j^{m,m+1}$ to obtain

$$\begin{aligned} \|z - \eta_j^{m,m+1}z\|_a & \leq \|z\|_{a(K_{j,m+1})} + \|z\|_{s(K_{j,m+1})} \\ & \leq (1 + \frac{1}{\sqrt{\Lambda}}) \|z\|_{a(K_{j,m+1})} + \|\pi z\|_{s(K_{j,m+1})}. \\ \|\pi(z - \eta_j^{m,m+1}z)\|_s & \leq \|z - \eta_j^{m,m+1}z\|_s \leq \|z\|_{s(K_{j,m+1})} \\ & \leq \frac{1}{\sqrt{\Lambda}} \|z\|_{a(K_{j,m+1})} + \|\pi z\|_{s(K_{j,m+1})}. \end{aligned}$$

By using the above, we can obtain the following estimates of I_1 and I_2 , which is

$$I_1 + I_2 \leq C(\Lambda) (\|z_j\|_a + \|\pi z_j\|_s) (\|z\|_{a(K_{j,m+1})} + \|\pi z\|_{s(K_{j,m+1})}).$$

Due to the following estimates

$$\|z_j\|_s \leq \|z_j - \pi z_j\|_s + \|\pi z_j\|_s \leq \frac{1}{\sqrt{\Lambda}} \|z_j\|_a + \|\pi z_j\|_s,$$

then for I_3

$$I_3 \leq C(\Lambda) (\|z_j\|_a + \|\pi z_j\|_s) (\|z\|_{a(K_{j,m+1})} + \|\pi z\|_{s(K_{j,m+1})}).$$

Also,

$$k^2 \|z_j\|^2 \leq c_* H^2 k^2 \varepsilon^{-2} \|z_j\|_s^2 \leq \frac{1}{2} \|z_j\|_s^2 \leq \frac{1}{2} \left(\frac{1}{\Lambda} \|z_j\|_a^2 + \|\pi z_j\|_s^2 \right).$$

and

$$\begin{aligned} k^2 \|z - \eta_j^{m,m+1} z\|^2 &\leq c_* H^2 k^2 \varepsilon^{-2} \|z - \eta_j^{m,m+1} z\|_s^2 \leq \frac{1}{2} \|z\|_{s(K_j, m+1)}^2 \\ &\leq \frac{1}{2\Lambda} \|z\|_{a(K_j, m+1)}^2 + \frac{1}{2} \|\pi z\|_{s(K_j, m+1)}^2, \end{aligned}$$

we can derive the last estimate for I_4 ,

$$I_4 \leq C(\Lambda) (\|z_j\|_a^2 + \|\pi z_j\|_s^2)^{1/2} (\|z\|_{a(K_j, m+1)}^2 + \|\pi z\|_{s(K_j, m+1)}^2)^{1/2}.$$

249 Collecting all the estimates of I_1 to I_4 , we hence obtain

$$|\mathcal{B}(z_j, z) + s(\pi z_j, \pi z)| \leq C(\Lambda) (\|z\|_{a(K_j, m+1)}^2 + \|\pi z\|_{s(K_j, m+1)}^2)^{1/2} (\|z_j\|_a^2 + \|\pi z_j\|_s^2)^{1/2}.$$

250 Recalling the definition of C_{ol} , it is easy to show

$$\sum_{j=1}^N (\|z\|_{a(K_j, m+1)}^2 + \|\pi z\|_{s(K_j, m+1)}^2) \leq C_{\text{ol}} (m+1)^d (\|z\|_a^2 + \|\pi z\|_s^2).$$

251 Meanwhile, we get

$$\|z\|_a^2 + \|\pi z\|_s^2 = \mathcal{B}(z, z) + s(\pi z, \pi z) + k^2(z, z) + ik(z, z)_\Gamma.$$

Taking the real part and the absolute value of the above and using the similar tricks from before,

$$|\text{Re}(ik(z, z)_\Gamma)| = 0, \quad |k^2(z, z)| \leq c_* k^2 H^2 \varepsilon^{-2} \|z\|_s^2 \leq \frac{1}{2} \left(\frac{1}{\Lambda} \|z\|_a^2 + \|\pi z\|_s^2 \right).$$

252 Then

$$\left(1 - \frac{1}{2\Lambda} \right) \|z\|_a^2 + \frac{1}{2} \|\pi z\|_s^2 \leq |\mathcal{B}(z, z) + s(\pi z, \pi z)|.$$

253 We also need to choose $\Lambda > \frac{1}{2}$ to obtain

$$\|z\|_a^2 + \|\pi z\|_s^2 \leq C(\Lambda) |\mathcal{B}(z, z) + s(\pi z, \pi z)|. \quad (17)$$

254 Finally, we can derive the global estimates

$$\begin{aligned}
\|z\|_a^2 + \|\pi z\|_s^2 &\leq C(\Lambda) |\mathcal{B}(z, z) + s(\pi z, \pi z)| \\
&\leq C(\Lambda) \left| \sum_{j=1}^N \mathcal{B}(z_j, z) + s(\pi z_j, \pi z) \right| \\
&\leq C(\Lambda) \sum_{j=1}^N |\mathcal{B}(z_j, z) + s(\pi z_j, \pi z)| \\
&\leq C(\Lambda) \left\{ \sum_{j=1}^N (\|z_j\|_a^2 + \|\pi z_j\|_s^2) \right\}^{1/2} \left\{ \sum_{j=1}^N (\|z\|_{a(K_j, m+1)}^2 + \|\pi z\|_{s(K_j, m+1)}^2) \right\}^{1/2} \\
&\leq C(\Lambda) \{C_{\text{ol}}(m+1)^d (\|z\|_a^2 + \|\pi z\|_s^2)\}^{1/2} \\
&\quad \left\{ C(\Lambda) \beta^m \sum_{j=1}^N (\|T_j t_j\|_a^2 + \|\pi T_j t_j\|_s^2) \right\}^{1/2} \\
&\leq C(\Lambda) \{C_{\text{ol}}(m+1)^d (\|z\|_a^2 + \|\pi z\|_s^2)\}^{1/2} \\
&\quad \left\{ C(\Lambda) \beta^m \sum_{j=1}^N |\mathcal{B}(T_j t_j, T_j t_j) + s(\pi T_j t_j, \pi T_j t_j)| \right\}^{1/2},
\end{aligned}$$

where the last inequality comes from the lemma 4.5 and eq. (17) by substituting z to $T_j t_j$. By using the previous results

$$\mathcal{B}(T_j t_j, T_j t_j) + s(\pi T_j t_j, \pi T_j t_j) = s(\pi t_j, \pi T_j t_j) \leq \|\pi t_j\|_s^2,$$

255 we can obtain the desired proof. \square

Next, we are going to prove that the global basis functions are indeed localizable. For this purpose, we need to define a bubble function $B(x)$ satisfies the following: for each coarse block $K_j \in \mathcal{T}_H$, then

$$\begin{cases} B(x) > 0, & \forall x \in \text{int}(K_j), \\ B(x) = 0, & \forall x \in \partial K_j. \end{cases}$$

We take $B = \Pi_j \eta_j$ where the product is taken over all vertices j on ∂K_j . Using the bubble function, we define the following constant

$$C_\pi = \sup_{K \in \mathcal{T}, \mu \in V_{\text{aux}}} \frac{\int_K \tilde{\kappa} \mu^2 dx}{\int_K B \tilde{\kappa} \mu^2 dx}.$$

256 In the following, we are going to prove lemma 4.7, which says that for any
 257 $\psi \in V_{\text{aux}}$, we can find a function ϕ in the space V such that the a -norm of the
 258 function ϕ is controlled by the s -norm of ψ and the support of the function
 259 ϕ is contained in the support of the function ψ .

Lemma 4.7. *For all $v_{\text{aux}} \in V_{\text{aux}}$, there exists a function $v \in H_0^1(\Omega)$ such that*

$$\pi(v) = v_{\text{aux}}, \quad \|v\|_a \leq C \|v_{\text{aux}}\|_s^2, \quad \text{supp}(v) \subset \text{supp}(v_{\text{aux}}).$$

Proof. Consider the space $V_{\text{aux}}(K_j)$ and $\psi \in V_{\text{aux}}(K_j)$, then we need to find $\phi \in V(K_j)$ and $\lambda \in V_{\text{aux}}$ such that

$$\begin{aligned} \int_{K_j} A \nabla \psi \cdot \nabla \bar{p} \, dx + \int_{K_j} \tilde{\kappa} p \bar{\lambda} \, dx &= 0 & \forall p \in V(K_j), \\ \int_{K_j} \tilde{\kappa} \psi \bar{q} \, dx &= \int_{K_j} \tilde{\kappa} \phi \bar{q} \, dx & \forall q \in V_{\text{aux}}(K_j). \end{aligned}$$

260 The above two equations is equivalent to the following minimization problem
 261 defined on the coarse block K_j : for a given $\psi \in V_{\text{aux}}^j$ with $\|\psi\| = 1$, then

$$\phi = \text{argmin} \{ a(w, w) \mid w \in V_0(K_j), s_j(w, \psi) = 1, s_j(w, m) = 0, \forall m \in V_{\text{aux}}^\perp \}. \quad (18)$$

The well-posedness of the problem eq. (18) is equivalent to the existence of a function $\phi \in V_0(K_j)$ such that

$$s_j(\phi, \psi) \geq C \|\psi\|_s^2, \quad \|\phi\|_{a(K_j)} \leq C \|\psi\|_{s(K_j)},$$

where C is independent of the meshsize but possibly depends on the problem parameters. Note that ψ is supported in K_j . We let $\phi = B\psi$. By the definition of s_j , we have

$$s_j(\psi, \phi) = \int_{K_j} \tilde{\kappa} B |\psi|^2 \, dx \geq C_\pi^{-1} \|\psi\|_{s(K_j)}^2.$$

Since

$$\nabla(B\psi) = \psi \nabla B + B \nabla \psi, \quad |B| \leq 1, \quad |\nabla B| \leq C_T \sum_j |\nabla \eta_j|^2,$$

then we have

$$\|\phi\|_{a(K_j)}^2 = \|B\psi\|_{a(K_j)}^2 \leq C_T C_\pi \|\phi\|_{a(K_j)} (\|\psi\|_{a(K_j)} + \|\psi\|_{s(K_j)}).$$

Finally, using the spectral problem eq. (5), we can obtain

$$\|\psi\|_{a(K_j)}^2 \leq \left(\max_{1 \leq i \leq l_j} \lambda_i^j \right) \|\psi\|_{s(K_j)}.$$

262 This proves the unique solvability of the minimization problem eq. (18). \square

263 The following lemma gives the well-posedness of the multiscale problem
264 eq. (12) by proving the inf-sup condition.

265 **Theorem 4.8.** *Under the resolution condition in lemma 4.1 and the over-*
266 *sampling condition $m \geq |\log(k\varepsilon^{-1})|$, the bilinear form \mathcal{B} satisfies the follow-*
267 *ing inf-sup condition: there exists a constant $\gamma_{\text{cem}} > 0$ depends on k such*
268 *that*

$$\inf_{u_H \in V_{\text{ms}}} \sup_{v_H^* \in V_{\text{ms}}^*} \frac{\text{Re} \mathcal{B}(u_H, v_H^*)}{\|u_H\|_{1,A,k} \|v_H^*\|_{1,A,k}} \geq \gamma_{\text{cem}}.$$

Proof. For $u_H \in V_{\text{ms}}$, we can find $u_H = T_m \psi$. Next we choose $u'_H = T\psi \in V_{\text{glo}}$. Recalling the inf-sup stability on V_{glo} and V_{glo}^* , we can find $v'_H = T^* \phi \in V_{\text{glo}}^*$ such that $\text{Re} \mathcal{B}(u'_H, v'_H) \geq \gamma \|u'_H\|_{1,A,k} \|v'_H\|_{1,A,k}$. Similarly, if we denote $v_H = T_m^* \phi$, we have Then we have

$$\begin{aligned} \mathcal{B}(u_H, v_H) &= \mathcal{B}(u'_H, v'_H) + \mathcal{B}(u'_H, v_H - v'_H) + \mathcal{B}(u_H - u'_H, v_H) \\ \text{Re} \mathcal{B}(u_H, v_H) &= \text{Re} \mathcal{B}(u'_H, v'_H) + \text{Re} \mathcal{B}(u'_H, v_H - v'_H) + \text{Re} \mathcal{B}(u_H - u'_H, v_H) \\ &\geq \gamma \|u'_H\|_{1,A,k} \|v'_H\|_{1,A,k} - \|u'_H\|_{1,A,k} \|v_H - v'_H\|_{1,A,k} \\ &\quad - \|u_H - u'_H\|_{1,A,k} \|v_H\|_{1,A,k} \\ &\geq \gamma \|u'_H\|_{1,A,k} \|v'_H\|_{1,A,k} - \|u'_H\|_{1,A,k} \|(T^* - T_m^*)\phi\|_{1,A,k} \\ &\quad - \|(T - T_m)\psi\|_{1,A,k} \|v_H\|_{1,A,k}. \end{aligned}$$

The next we need to show that

$$\|(T^* - T_m^*)\phi\|_{1,A,k} \leq \|T^* \phi\|_{1,A,k} \text{ and } \|(T - T_m)\psi\|_{1,A,k} \leq \|T\psi\|_{1,A,k}.$$

Combining lemma 4.6 to obtain

$$\|(T_m - T)\psi\|_a^2 + k^2 \|(T_m - T)\psi\|^2 \leq C(\Lambda) \sqrt{C_{\text{ol}} \beta^{m/2}} (m+1)^{d/2} \|\pi\psi\|_s^2.$$

269 where we use the resolution condition

$$k^2 \|(T_m - T)\psi\|^2 \leq c_* k^2 H^2 \varepsilon^{-2} \|(T_m - T)\psi\|_s^2 \leq \frac{1}{2\Lambda} \|(T_m - T)\psi\|_a^2 + \|\pi(T_m - T)\psi\|_s^2.$$

Our remaining task is to $\|\pi\psi\|_s$ can be bounded by $\|T\psi\|_a$ due to the following

$$\|\pi\psi\|_s^2 + k^2\|T\psi\|^2 \leq \|T\psi\|_a^2 + k^2\|T\psi\|^2 = \|T\psi\|_{1,A,k}^2.$$

Take ψ as the test function, we can obtain

$$\mathcal{B}(T\psi, \psi) + s(\pi T\psi, \pi\psi) = s(\pi\psi, \pi\psi).$$

Then

$$\begin{aligned} \|\pi\psi\|_s^2 &\leq \|T\psi\|_{1,A,k}\|\psi\|_{1,A,k} + \|\pi T\psi\|_s\|\pi\psi\|_s \\ &\leq (\|T\psi\|_a^2 + k^2\|T\psi\|^2)^{1/2}(\|\psi\|_a^2 + k^2\|\psi\|^2)^{1/2} + \|\pi T\psi\|_s\|\pi\psi\|_s. \end{aligned}$$

270 We again use the resolution condition

$$\begin{aligned} k^2\|T\psi\|^2 &\leq c_*k^2H^2\varepsilon^{-2}\|T\psi\|_s^2 \leq \frac{1}{2\Lambda}\|T\psi\|_a^2 + \|\pi T\psi\|_s^2, \\ k^2\|\psi\|^2 &\leq c_*k^2H^2\varepsilon^{-2}\|\psi\|_s^2 \leq \frac{1}{2\Lambda}\|\psi\|_a^2 + \|\pi\psi\|_s^2. \end{aligned}$$

By using the fact in lemma 4.7 to obtain $\|\psi\|_a \leq \|\pi\psi\|_s$, finally we can obtain

$$\begin{aligned} \|\pi\psi\|_s^2 &\leq \|T\psi\|_{1,A,k}\|\psi\|_{1,A,k} + \|\pi T\psi\|_s\|\pi\psi\|_s \\ &\leq (C(\Lambda)\|T\psi\|_a^2 + \|\pi T\psi\|_s^2)^{1/2}C(\Lambda)\|\pi\psi\|_s + \|\pi T\psi\|_s\|\pi\psi\|_s. \end{aligned}$$

Meanwhile, utilizing Poincare inequality, we can obtain

$$\|\pi T\psi\|_s \leq \|T\psi\|_s \leq C_{\text{po}}H^{-1}\|T\psi\|_a.$$

Then we obtain the desired estimate

$$\|(T_m - T)\psi\|_a + k^2\|(T_m - T)\psi\| \leq C(\Lambda)H^{-1}\sqrt{C_{\text{ol}}}\beta^{m/2}(m+1)^{d/2}\|T\psi\|_{1,A,k}.$$

Using the same tricks to obtain

$$\|(T_m^* - T^*)\phi\|_a + k^2\|(T_m^* - T^*)\phi\| \leq C(\Lambda)H^{-1}\sqrt{C_{\text{ol}}}\beta^{m/2}(m+1)^{d/2}\|T^*\phi\|_{1,A,k}.$$

Finally we obtain

$$\text{Re } \mathcal{B}(u_H, v_H^*) \geq (\gamma - 2C(\Lambda)H^{-1}\sqrt{C_{\text{ol}}}\beta^{m/2}(m+1)^{d/2})\|u_H\|_{1,A,k}\|v_H^*\|_{1,A,k}.$$

271

□

272 **Theorem 4.9.** *Let u be the solution of the problem eq. (1) and u_{ms} be the*
 273 *solution of the multiscale problem eq. (12). Then we have*

$$\|u - u_{\text{ms}}\|_a \leq \frac{1}{\varepsilon_0 \sqrt{\Lambda}} \|f\|_{s-1} + C(\Lambda) \sqrt{C_{\text{ol}}} \beta^{m/2} (m+1)^{d/2} (C_{\text{inv}} \|u^{\text{glo}}\|_a + \|\pi u^{\text{glo}}\|_s).$$

Proof. Denote $e := u - u_{\text{ms}}$, the triangle inequality gives

$$\|e\|_a^2 \leq \|u - u_{\text{glo}}\|_a^2 + \|u_{\text{glo}} - u_{\text{ms}}\|_a^2 \leq \frac{1}{\varepsilon_0 \sqrt{\Lambda}} \|f\|_{s-1} + \|u_{\text{glo}} - u_{\text{ms}}\|_a^2,$$

where lemma 4.3 is applied to the first term of above. The next we estimate the remaining term $\|u_{\text{glo}} - u_{\text{ms}}\|_a$. Due to the Cea's Lemma, there exist ψ_* , ψ'_* such that $u_{\text{glo}} = T\psi_*$, $u_{\text{ms}} = T_m\psi'_*$, and

$$\|T\psi_* - T_m\psi'_*\|_{1,A,k} \leq \inf_{\psi''_* \in V} \|T\psi_* - T_m\psi''_*\|_{1,A,k}.$$

Then, choose $\psi''_* = \psi_* \in V$, then

$$\|u_{\text{glo}} - u_{\text{ms}}\|_{1,A,k}^2 \leq \|(T - T_m)\psi_*\|_{1,A,k}^2 = \|(T - T_m)\psi_*\|_a^2 + k^2 \|(T - T_m)\psi_*\|_s^2.$$

274 Using the resolution condition

$$\begin{aligned} k^2 \|(T - T_m)\psi_*\|_s^2 &\leq c_* k^2 H^2 \varepsilon^{-2} \|(T - T_m)\psi_*\|_s^2 \\ &\leq \frac{1}{2\Lambda} \|(T - T_m)\psi_*\|_a^2 + \|\pi(T - T_m)\psi_*\|_s^2. \end{aligned}$$

By using the same tricks in proving lemma 4.6 to obtain

$$\|(T - T_m)\psi_*\|_a^2 + \|\pi(T - T_m)\psi_*\|_s^2 \leq C^2(\Lambda) C_{\text{ol}} \beta^m (m+1)^d \|\pi\psi_*\|_s^2.$$

Then we let $v = \psi_*$ and to obtain

$$\|\pi\psi_*\|_s^2 = \mathcal{B}(u^{\text{glo}}, \psi_*) + s(\pi u^{\text{glo}}, \pi\psi_*).$$

According to lemma 4.7, it is possible to find $\hat{\psi}_* \in V$ such that $\hat{\psi}_* = \pi\psi_*$ and $\|\hat{\psi}_*\|_a \leq C_{\text{inv}} \|\pi\psi_*\|_s$. Recalling the definition of the operator \mathcal{B}

$$\mathcal{B}(u^{\text{glo}}, \hat{\psi}_*) = a(u^{\text{glo}}, \hat{\psi}_*) - k^2(u^{\text{glo}}, \hat{\psi}_*) - ik(u^{\text{glo}}, \hat{\psi}_*)_{\Gamma}.$$

275 For the second term on the right hand side, using the resolution condition

$$\begin{aligned} \left| k^2(u^{\text{glo}}, \hat{\psi}_*) \right| &\leq c_* k^2 H^2 \varepsilon^{-2} \|u^{\text{glo}}\|_s \|\hat{\psi}_*\|_s \\ &\leq \frac{1}{2} \left(\frac{1}{\sqrt{\Lambda}} \|u^{\text{glo}}\|_a + \|\pi u^{\text{glo}}\|_s \right) \left(\frac{1}{\sqrt{\Lambda}} \|\hat{\psi}_*\|_a + \|\pi \hat{\psi}_*\|_s \right). \end{aligned}$$

276 Similarly,

$$\begin{aligned} \left| \mathbf{i}k(u^{\text{glo}}, \hat{\psi}_*)_\Gamma \right| &\leq \|u^{\text{glo}}\|_{1,A,k} \|\hat{\psi}_*\|_{1,A,k} \\ &\leq (\|u^{\text{glo}}\|_a^2 + k^2 \|u^{\text{glo}}\|^2)^{1/2} (\|\hat{\psi}_*\|_a^2 + k^2 \|\hat{\psi}_*\|^2)^{1/2} \\ &\leq \left(\|u^{\text{glo}}\|_a^2 + \frac{1}{2} \left(\frac{1}{\Lambda} \|u^{\text{glo}}\|_a^2 + \|\pi u^{\text{glo}}\|_s^2 \right) \right)^{1/2} \\ &\quad \left(\|\hat{\psi}_*\|_a^2 + \frac{1}{2} \left(\frac{1}{\Lambda} \|\hat{\psi}_*\|_a^2 + \|\pi \hat{\psi}_*\|_s^2 \right) \right)^{1/2}. \end{aligned}$$

277 All in all, we can obtain

$$\|\pi \psi_*\|_s^2 \leq \|\pi \psi_*\|_s (C_{\text{inv}} \|u^{\text{glo}}\|_a + C \|\pi u^{\text{glo}}\|_s).$$

278

□

279 Moreover, it is easy to obtain $\|f\|_{s-1} = O(H)$. From the inf-sup condition
280 of the global problem in lemma 4.2 and eq. (13), we obtain for any $v \in V_{\text{glo}}^* \subset$
281 H^1 ,

$$\sup_{v \in H^1} \frac{(f, v)}{\|v\|_{1,A,k}} \geq \gamma(k) \|u^{\text{glo}}\|_{1,A,k}. \quad (19)$$

By using Cauchy–Schwartz inequality and the definition of the k -weighted norm, we obtain from eq. (19),

$$\gamma(k) \|f\| \geq \|u^{\text{glo}}\|_{1,A,k}.$$

Due to

$$\|u^{\text{glo}}\|_{1,A,k}^2 = \|u^{\text{glo}}\|_a^2 + k^2 \|u^{\text{glo}}\|^2 \leq \gamma^2(k) \|f\|^2,$$

282 we choose $\gamma(k) = k^{-1}$ to obtain

$$\|u^{\text{glo}}\|_a + \|\pi u^{\text{glo}}\|_s \leq \|u^{\text{glo}}\|_a + H^{-1} \|u^{\text{glo}}\| \leq O(k^{-1}) + O((kH)^{-1}).$$

If we assume $C_{\text{inv}} = O(1)$ and choose suitable m such that $\beta^{m/2}(m+1)^{d/2} = O((kH)^2)$, we will have

$$\|u - u_{\text{ms}}\|_a = O(kH).$$

283 **5. Numerical experiments**

284 In this section, we provide several examples of Helmholtz equations in dif-
 285 ferent domains solved by using CEM-GMsFEM method, which demonstrates
 286 our established theoretical analysis. We let u_h denotes the reference solution
 287 and let e_h denotes the error between the reference solution and numerical
 288 solution. The accuracy will be measured both in the L^2 norm and energy
 289 norm:

$$e_{L^2} := \frac{\|e_h\|_{L^2(\Omega)}}{\|u_h\|_{L^2(\Omega)}}, \quad e_a := \frac{\|e_h\|_{a(\Omega)}}{\|u_h\|_{a(\Omega)}}.$$

290 In order to clearly state the experimental results, we list the notations in the
 291 following table 1.

292 We conduct all numerical experiments on a square domain $\Omega = [0, 1] \times$
 293 $[0, 1]$. We will calculate reference solutions on a 200×200 mesh with the
 294 bilinear Lagrange FEM, therefore the media term $A(x)$ is generated from
 295 $200\text{px} \times 200\text{px}$ figures. For the coarse grid, we choose H to be $1/10, 1/20$
 296 and $1/40$. For simplicity, we take \tilde{A} as $\tilde{A}|_{K_j} = 24H^{-2}A|_{K_j}$ for all numerical
 297 experiments as suggested in [35] and we implement all simulations using the
 Python libraries Numpy and SciPy.

Table 1: Simplified description of symbols

Parameters	Symbols
Number of oversampling layers	m
Number of basis functions in every coarse element	N_{bf}
Length of every coarse element size	H
Length of every fine element size	h

298

299 *5.1. Model problem 1*

300 In the first model, we consider about the following Helmholtz equation
 301 in with the boundary and the source term $f(\vec{x}) = 0$. Then we obtained the
 302 following equation from eq. (1)

$$\begin{cases} -\nabla \cdot (A(x_1, x_2)\nabla u) - k^2u = 0 & \forall (x_1, x_2) \in \Omega, \\ A(x_1, x_2)\nabla u \cdot \mathbf{n} - ik u = g(x_1, x_2) & \forall (x_1, x_2) \in \partial\Omega, \end{cases} \quad (20)$$

303 We firstly consider about the homogeneous coefficients $A(\vec{x}) = I$ with wave
 304 number $k = 2^4$. The boundary data g is chosen in eq. (21) such that the

305 problem admits the plane wave solution $u_* = \exp(i\vec{k} \cdot \vec{x})$ with $\vec{k} = k(0.6, 0.8)$.

$$g(x_1, x_2) = \begin{cases} -i1.6k \cdot \exp(ik \cdot 0.8x_2), & \text{on } \{0\} \times (0, 1), \\ -i0.4k \cdot \exp(ik \cdot (0.6 + 0.8x_2)), & \text{on } \{1\} \times (0, 1), \\ -i1.8k \cdot \exp(ik \cdot 0.6x_1), & \text{on } (0, 1) \times \{0\}, \\ -i0.2k \cdot \exp(ik \cdot (0.6x_1 + 0.8)), & \text{on } (0, 1) \times \{1\}. \end{cases} \quad (21)$$

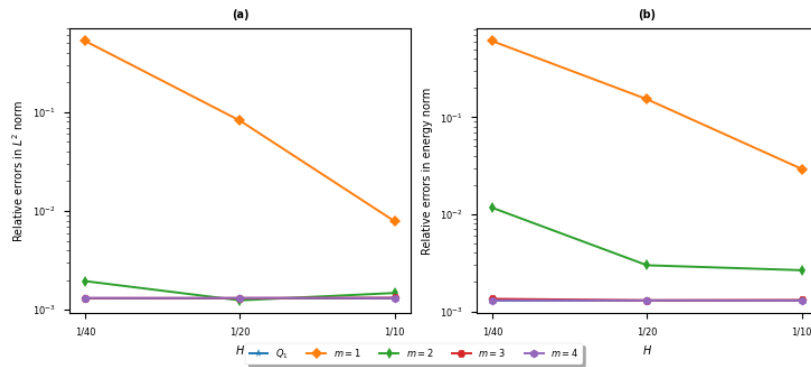


Figure 2: Numerical results for the Helmholtz equations with homogeneous coefficients where the relative errors of the proposed method with different numbers of oversampling layers m and the Q_1 FEM are calculated with respect to the coarse mesh size H . Subplots (a) and (b) which the relative errors are measured in the L_2 norm and energy norm, respectively.

H	N_{bf}	m	$\ u_{\text{cem}} - u_h\ _{L^2(\Omega)}$	$\ u_{\text{cem}} - u_h\ _{a(\Omega)}$
1/10	4	2	1.32e-02	1.30e-02
1/20	4	3	1.25e-03	1.54e-02
1/40	4	4	1.92e-04	3.97e-03

Table 2: Numerical errors of CEM-GMsFEM using 4 basis functions in each coarse mesh with the oversampling layers equal to m . Errors in the L^2 norm and energy norm with different H .

306

307 For the setting of the proposed multiscale method, we fix $l_j = 4$, indicat-
 308 ing that we calculate the first four eigenfunctions in eq. (5) and construct
 309 four multiscale bases for each coarse element, while we vary the oversampling
 310 layers m from 1 to 4. With regard to the relative error norms, we choose u_h

311 to be the exact solution of the Helmholtz equation with the homogeneous
 312 coefficients and u_{cem} is approximated by the CEM-GMsFEM method and e_h
 313 represents the difference between the u_h and u_{cem} . In order to show the effi-
 314 cient of our multiscale method, we also shows the relative error between the
 315 exact solution and the approximated solution which is obtained from the $Q1$
 316 FEM. We can observe from subplots (a) to (b) in fig. 2 that the convergence
 317 of the $Q1$ FEM manifests a linear pattern with respect to H in the logarith-
 318 mic scale, consistent with the theoretical expectation. We can also see that
 319 the number of oversampling layers m has a significant impact on the accuracy
 320 of the proposed method and the results of the relative errors with respect to
 321 different mesh size and oversampling layers are shown in table 2. However,
 322 for the same m , the error decaying with respect to H does not always hold
 323 ($m = 1, 2$), as depicted in subplots (a) and (b). Although for $m = 3, 4$, the
 324 proposed method exhibits higher accuracy than the $Q1$ FEM, the compu-
 325 tational cost is significantly same or higher due to the sophisticated process
 326 of constructing multiscale bases. Therefore, the proposed method is more
 327 suitable for scenarios involving intricate coefficient profiles.

328 *5.2. Model problem 2*

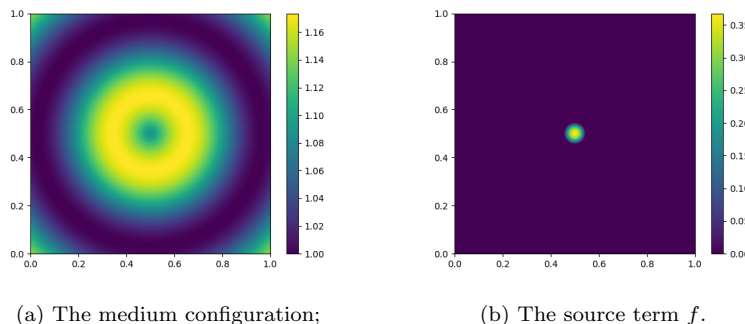


Figure 3: Model Problem 2

329 In the second model, we consider about the following Helmholtz equation
 330 with pointwise isotropic coefficients $A(x_1, x_2)$ displayed in fig. 3a and source
 331 term f is chosen in eq. (22) and it is shown in fig. 3b.

$$f(x_1, x_2) = \begin{cases} \exp\left(-\frac{1}{1-400(x_1^2+x_2^2)}\right) & \text{for } \sqrt{x_1^2 + x_2^2} < 1/20, \\ 0 & \text{else.} \end{cases} \quad (22)$$

332 Then we obtained the following equation from eq. (1)

$$\begin{cases} -\nabla \cdot (A(x_1, x_2)\nabla u) - k^2 u = f(x_1, x_2) & \forall (x_1, x_2) \in \Omega, \\ A(x_1, x_2)\nabla u \cdot \mathbf{n} - iku = 0 & \forall (x_1, x_2) \in \partial\Omega. \end{cases} \quad (23)$$

H	N_{bf}	m	$\ u_{\text{cem}} - u_h\ _{L^2(\Omega)}$	$\ u_{\text{cem}} - u_h\ _{a(\Omega)}$
1/10	4	2	1.80e-02	8.24e-02
1/20	4	3	1.00e-03	9.27e-03
1/40	4	4	1.03e-04	1.87e-03

Table 3: Numerical errors of CEM-GMsFEM using 4 basis functions in each coarse mesh with the oversampling layers equal to m . Errors in the L^2 norm and energy norm with different H .

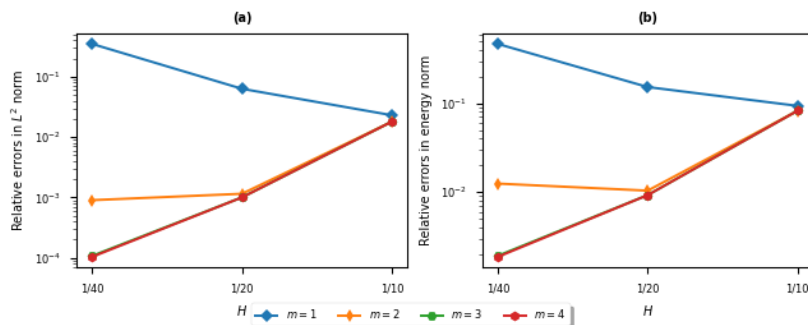


Figure 4: Subplots (a) and (b) show the relative errors of the proposed method for the pointwise isotropic coefficients with different numbers of oversampling layers m with respect to the coarse mesh size H , but measured in different norms.

333

334 The numerical results of the $Q1$ FEM and the proposed method with
 335 $m \in \{1, 2, 3\}$ are presented in fig. 4 where Subplots (a) and (b) in fig. 4 share
 336 the same setting (corresponding to the fig. 2) and the relative errors are
 337 measured in the different norms. We choose u_h to be the $Q1$ FEM solution
 338 and u_{cem} is approximated by the CEM-GMsFEM method and e_h represents
 339 the difference between the u_h and u_{cem} , which are shown in fig. 5. The
 340 classical CEM-GMsFEM [28] is proven to be effective in handling long and
 341 high-contrast channels, and the proposed method inherits this advantage.
 342 By setting $m = 3, 4$, the proposed method can achieve a relative error of

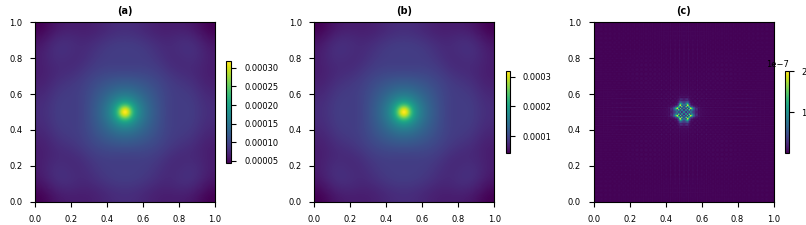


Figure 5: Solutions by using $H = 1/40$ and oversampling layer equals to 3. Subplot (a), (b),(c) represent reference solution , CEM-GMsFEM solution and Difference of these two solutions, respectively .

343 10% in the energy norm. Typically, the relative errors in the L_2 norm are
 344 significantly smaller by an order of magnitude than those in the energy norm,
 345 and the proposed method can achieve a relative error of 0.015 in the L_2 norm
 346 for $m = 3$. Furthermore, comparing subplots (a) and (b) reveals similar
 347 convergence behavior, indicating that the scale of the models does not affect
 348 the accuracy of the proposed method. We also list results of the relative
 349 errors with respect to different mesh size and oversampling layers are shown
 350 in table 3. Note that we solve the Helmholtz equation in coarser mesh, which
 351 means we can solve the issues of the pollution effect.

352 5.3. Model problem 3

H	N_{bf}	m	$\ u_{\text{cem}} - u_h\ _{L^2(\Omega)}$	$\ u_{\text{cem}} - u_h\ _{a(\Omega)}$
1/10	4	2	0.9935	0.9981
1/20	4	3	0.8260	0.8361
1/40	4	4	0.0126	0.0213

Table 4: Numerical errors of CEM-GMsFEM using 4 basis functions in each coarse mesh with the oversampling layers equal to m . Errors in the L^2 norm and energy norm with different H .

353 In the third model, we make use of high-contrast coefficients $A(x_1, x_2)$ dis-
 354 played in fig. 6a with a 10^{-3} contrast ratio as the show case for the Helmholtz

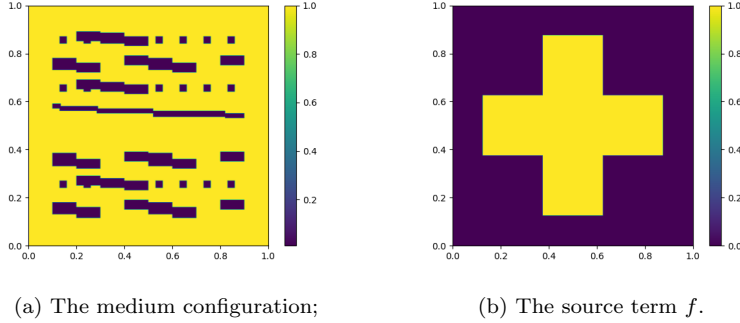


Figure 6: Model Problem 3

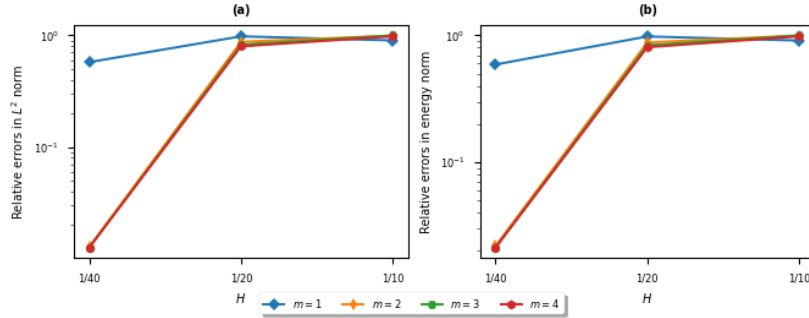


Figure 7: Subplots (a) and (b) show the relative errors of the proposed method for the high-contrast coefficients with different numbers of oversampling layers m w.r.t. the coarse mesh size H , but measured in different norms.

355 equation, and source term f is chosen as a piecewise constant function which
 356 is shown in fig. 6b. The numerical results of the proposed multiscale method
 357 with $m \in \{1, 2, 3, 4\}$ are presented in fig. 7 where subplots (a) and (b) in
 358 fig. 7 also share the same setting with the mesh size and wavenumber and
 359 the relative errors are measured in the different norms as well. We choose u_h
 360 to be the reference solution approximated by the $Q1$ FEM method due to the
 361 lack of the classical solution and e_h represents the difference between the mul-
 362 tiscale solution u_{cem} and $Q1$ FEM solution u_h , which are shown in fig. 8. The
 363 proposed method inherits this advantage of CEM-GMsFEM which is proven
 364 to be effective in handling long and high-contrast channels. Specifically, we
 365 outlines the errors in both L^2 and energy norms corresponding to different
 366 chosen m in table 4. By setting $m = 3, 4$, the proposed method can achieve a
 367 relative error of almost 2% in the energy norm. Typically, the relative errors

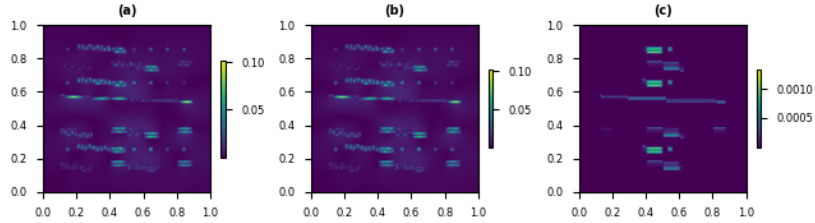


Figure 8: Solutions by using $H = 1/40$ and oversampling layer equals to 3. Subplot (a), (b),(c) represent reference solution , CEM-GMsFEM solution and difference of above two solutions, respectively.

368 in the L_2 norm are significantly smaller by an order of magnitude than those
 369 in the energy norm, and the proposed method can achieve a relative error
 370 of 1.2% in the L_2 norm for $m = 2, 3, 4$. Furthermore, comparing subplots
 371 (a) and (b) in fig. 7 reveals similar convergence behavior, indicating that the
 372 scale of the models does not affect the accuracy of the proposed method.

373 6. Conclusion

374 The paper introduces the CEM-GMsFEM method for solving Helmholtz
 375 equations in heterogeneous medium, provides the proof of convergence for
 376 this method, and presents numerical experiments to support its effectiveness.
 377 The work contributes to the field by offering a novel approach to tackle
 378 heterogeneous Helmholtz problems without restrictive assumptions on the
 379 coefficient structures.

380 In future work, we plan to apply the CEM-GMsFEM method to solve
 381 Helmholtz equations in other types of domains or in more complex geometries,
 382 such as perforated domains. Perforated domains are characterized by
 383 having small holes or voids within the domain, and their inclusion introduces
 384 additional challenges in accurately capturing the solution behavior.
 385 Additionally, we are also interested in exploring more efficient techniques to
 386 solve Helmholtz equations with much higher frequencies. These future directions
 387 would contribute to advancing the field of multiscale modeling and
 388 simulation of Helmholtz equations in diverse and challenging scenarios.

389 **7. Acknowledgment**

390 The research of Eric Chung is partially supported by the Hong Kong RGC
391 General Research Fund (Projects: 14305423 and 14305222).

392 **References**

- 393 [1] B. A. Romanowicz, Using seismic waves to image earth's inter-
394 nal structure, *Nature* 451 (2008) 266–268. URL: [https://api.
395 semanticscholar.org/CorpusID:518013](https://api.semanticscholar.org/CorpusID:518013).
- 396 [2] D. Lahaye, J. Tang, C. Vuik, *Modern Solvers for Helmholtz Problems*,
397 Birkhäuser, 2017. doi:10.1007/978-3-319-28832-1.
- 398 [3] I. M. Babuška, S. A. Sauter, Is the pollution effect of the fem avoidable
399 for the helmholtz equation considering high wave numbers?, *SIAM Jour-
400 nal on Numerical Analysis* 34 (1997) 2392–2423. URL: [https://doi.
401 org/10.1137/S003614294269186](https://doi.org/10.1137/S003614294269186). doi:10.1137/S0036142994269186.
402 arXiv:<https://doi.org/10.1137/S0036142994269186>.
- 403 [4] F. Ihlenburg, I. Babuska, Finite element solution of the helmholtz equa-
404 tion with high wave number part ii: The h-p version of the fem, *SIAM
405 Journal on Numerical Analysis* 34 (1997) 315–358. URL: [https://doi.
406 org/10.1137/S0036142994272337](https://doi.org/10.1137/S0036142994272337). doi:10.1137/S0036142994272337.
407 arXiv:<https://doi.org/10.1137/S0036142994272337>.
- 408 [5] L. Hervella-Nieto, P. M. López-Pérez, A. Prieto, Robustness and
409 dispersion analysis of the partition of unity finite element method
410 applied to the helmholtz equation, *Computers and Mathematics
411 with Applications* 79 (2020) 2426–2446. URL: [https://www.
412 sciencedirect.com/science/article/pii/S0898122119305425](https://www.sciencedirect.com/science/article/pii/S0898122119305425).
413 doi:<https://doi.org/10.1016/j.camwa.2019.11.009>.
- 414 [6] C. Chang, A least-squares finite element method for the helmholtz
415 equation, *Computer Methods in Applied Mechanics and En-
416 gineering* 83 (1990) 1–7. URL: [https://www.sciencedirect.com/
417 science/article/pii/0045782590901212](https://www.sciencedirect.com/science/article/pii/0045782590901212). doi:[https://doi.org/10.
418 1016/0045-7825\(90\)90121-2](https://doi.org/10.1016/0045-7825(90)90121-2).

- 419 [7] T. Strouboulis, I. Babuška, R. Hidajat, The generalized finite element
420 method for helmholtz equation: Theory, computation, and open prob-
421 lems, *Computer Methods in Applied Mechanics and Engineering* 195
422 (2006) 4711–4731. URL: [https://www.sciencedirect.com/science/
423 article/pii/S0045782505005037](https://www.sciencedirect.com/science/article/pii/S0045782505005037). doi:[https://doi.org/10.1016/j.
424 cma.2005.09.019](https://doi.org/10.1016/j.cma.2005.09.019), john H. Argyris Memorial Issue. Part I.
- 425 [8] H. Chen, P. Lu, X. Xu, A hybridizable discontinuous galerkin
426 method for the helmholtz equation with high wave number,
427 *SIAM Journal on Numerical Analysis* 51 (2013) 2166–2188. URL:
428 <https://doi.org/10.1137/120883451>. doi:10.1137/120883451.
429 arXiv:<https://doi.org/10.1137/120883451>.
- 430 [9] X. Feng, H. Wu, Discontinuous galerkin methods for the
431 helmholtz equation with large wave number, *SIAM Jour-
432 nal on Numerical Analysis* 47 (2009) 2872–2896. URL:
433 <https://doi.org/10.1137/080737538>. doi:10.1137/080737538.
434 arXiv:<https://doi.org/10.1137/080737538>.
- 435 [10] J. M. Melenk, S. Sauter, Convergence analysis for finite element dis-
436 cretizations of the helmholtz equation with dirichlet-to-neumann bound-
437 ary conditions, *Mathematics of Computation* 79 (2010) 1871–1914.
438 URL: <http://www.jstor.org/stable/20779130>.
- 439 [11] J. M. Melenk, S. Sauter, Wavenumber explicit convergence
440 analysis for galerkin discretizations of the helmholtz equation,
441 *SIAM Journal on Numerical Analysis* 49 (2011) 1210–1243. URL:
442 <https://doi.org/10.1137/090776202>. doi:10.1137/090776202.
443 arXiv:<https://doi.org/10.1137/090776202>.
- 444 [12] T. Y. H. Eric T. Chung, Yalchin Efendiev, *Multiscale Model Reduction:
445 Multiscale Finite Element Methods and Their Generalizations*, Springer
446 International Publishing, 2023.
- 447 [13] S. Fu, E. T. Chung, G. Li, Edge multiscale methods for elliptic problems
448 with heterogeneous coefficients, *Journal of Computational Physics* 396
449 (2019) 228–242. URL: [https://www.sciencedirect.com/science/
450 article/pii/S0021999119304139](https://www.sciencedirect.com/science/article/pii/S0021999119304139). doi:[https://doi.org/10.1016/j.
451 jcp.2019.06.006](https://doi.org/10.1016/j.jcp.2019.06.006).

- 452 [14] A. Målqvist, D. Peterseim, Localization of elliptic multiscale problems,
453 Mathematics of Computation 83 (2014) 2583–2603.
- 454 [15] D. Peterseim, B. Verfürth, Computational high frequency scattering
455 from high contrast heterogeneous media, Mathematics of Computation
456 89 (2019) 2649–2674. doi:<https://doi.org/10.1090/mcom/3529>.
- 457 [16] D. Peterseim, Eliminating the pollution effect in helmholtz problems by
458 local subscale correction, Math. Comput. 86 (2014) 1005–1036. URL:
459 <https://api.semanticscholar.org/CorpusID:32750126>.
- 460 [17] P. Freese, M. Hauck, D. Peterseim, Super-localized orthogonal de-
461 composition for high-frequency helmholtz problems, arXiv preprint
462 arXiv:2112.11368 (2021).
- 463 [18] D. L. Brown, D. Gallistl, D. Peterseim, Multiscale Petrov-
464 Galerkin method for high-frequency heterogeneous Helmholtz equations,
465 Springer, 2017.
- 466 [19] U. Gavrilieva, M. Vasilyeva, I. Harris, E. T. Chung, Y. Efendiev, Mul-
467 tiscale Finite Element Method for scattering problem in heterogeneous
468 domain, Journal of Physics: Conference Series 1392 (2019) 012067.
469 doi:<https://doi.org/10.48550/arXiv.1902.09935>.
- 470 [20] S. Fu, E. T. Chung, G. Li, An Edge Multiscale Interior Penalty Dis-
471 continuous Galerkin method for heterogeneous Helmholtz problems with
472 large varying wavenumber, Journal of Computational Physics 441 (2021)
473 110387. doi:<https://doi.org/10.1016/j.jcp.2021.110387>.
- 474 [21] M. Chupeng, C. Alber, R. Scheichl, Wavenumber explicit convergence
475 of a multiscale generalized finite element method for heterogeneous
476 helmholtz problems, SIAM Journal on Numerical Analysis 61 (2023)
477 1546–1584. URL: <https://doi.org/10.1137/21M1466748>. doi:10.
478 1137/21M1466748. arXiv:<https://doi.org/10.1137/21M1466748>.
- 479 [22] Y. Chen, T. Y. Hou, Y. Wang, Exponentially convergent multiscale
480 methods for 2d high frequency heterogeneous helmholtz equations, Mul-
481 tiscale Modeling & Simulation 21 (2023) 849–883.
- 482 [23] E. T. Chung, Y. Efendiev, W. T. Leung, Constraint Energy Minimizing
483 Generalized Multiscale Finite Element Method, Computer Methods in

- 484 Applied Mechanics and Engineering 339 (2018) 298–319. doi:[https://](https://doi.org/10.1016/j.cma.2018.04.010)
485 doi.org/10.1016/j.cma.2018.04.010.
- 486 [24] L. Zhao, E. T. Chung, Constraint Energy Minimizing Generalized Mul-
487 tiscale Finite Element Method for Convection Diffusion Equation, Mul-
488 tiscale Modeling & Simulation 21 (2023) 735–752. doi:[https://doi.](https://doi.org/10.1137/22M1487655)
489 [org/10.1137/22M1487655](https://doi.org/10.1137/22M1487655).
- 490 [25] Z. Wang, C. Ye, E. T. Chung, A multiscale method
491 for inhomogeneous elastic problems with high contrast coeffi-
492 cients, Journal of Computational and Applied Mathematics 436
493 (2024) 115397. URL: [https://www.sciencedirect.com/science/](https://www.sciencedirect.com/science/article/pii/S0377042723003412)
494 [article/pii/S0377042723003412](https://www.sciencedirect.com/science/article/pii/S0377042723003412). doi:[https://doi.org/10.1016/j.](https://doi.org/10.1016/j.cam.2023.115397)
495 [cam.2023.115397](https://doi.org/10.1016/j.cam.2023.115397).
- 496 [26] Y. Wang, E. T. Chung, L. Zhao, Constraint energy minimization
497 generalized multiscale finite element method in mixed formulation for
498 parabolic equations, Mathematics and Computers in Simulation 188
499 (2021) 455–475. URL: [https://www.sciencedirect.com/science/](https://www.sciencedirect.com/science/article/pii/S0378475421001348)
500 [article/pii/S0378475421001348](https://www.sciencedirect.com/science/article/pii/S0378475421001348). doi:[https://doi.org/10.1016/j.](https://doi.org/10.1016/j.matcom.2021.04.016)
501 [matcom.2021.04.016](https://doi.org/10.1016/j.matcom.2021.04.016).
- 502 [27] R. Altmann, P. Henning, D. Peterseim, Numerical homogenization be-
503 yond scale separation, Acta Numerica 30 (2021) 1–86. doi:[10.1017/](https://doi.org/10.1017/S0962492921000015)
504 [S0962492921000015](https://doi.org/10.1017/S0962492921000015).
- 505 [28] Y. Efendiev, J. Galvis, T. Y. Hou, Generalized multiscale finite element
506 methods (gmsfem), Journal of Computational Physics 251 (2013) 116–
507 135. URL: [https://www.sciencedirect.com/science/article/pii/](https://www.sciencedirect.com/science/article/pii/S0021999113003392)
508 [S0021999113003392](https://www.sciencedirect.com/science/article/pii/S0021999113003392). doi:[https://doi.org/10.1016/j.jcp.2013.04.](https://doi.org/10.1016/j.jcp.2013.04.045)
509 [045](https://doi.org/10.1016/j.jcp.2013.04.045).
- 510 [29] J. D. Joannopoulos, S. G. Johnson, J. N. Winn, R. D. Meade, Photonic
511 Crystals: Molding the Flow of Light - Second Edition, rev - revised, 2
512 ed., Princeton University Press, 2008. URL: [http://www.jstor.org/](http://www.jstor.org/stable/j.ctvc4gz9)
513 [stable/j.ctvc4gz9](http://www.jstor.org/stable/j.ctvc4gz9).
- 514 [30] R. Maier, Computational Multiscale Methods in Unstructured Hetero-
515 geneous Media, Ph.D. thesis, University of Augsburg, 2020.

- 516 [31] I. G. Graham, S. A. Sauter, Stability and error analysis
517 for the Helmholtz equation with variable coefficients, arXiv
518 preprint arXiv:1803.00966 (2018). doi:[https://doi.org/10.48550/
519 arXiv.1803.00966](https://doi.org/10.48550/arXiv.1803.00966).
- 520 [32] P. Grisvard, Elliptic Problems in Nonsmooth Domains, Society for
521 Industrial and Applied Mathematics, 2011. doi:[https://doi.org/10.
522 1137/1.9781611972030](https://doi.org/10.1137/1.9781611972030).
- 523 [33] D. Boffi, F. Brezzi, M. Fortin, Mixed Finite Element Methods and
524 Applications, volume 44, Springer Science & Business Media, 2013.
525 doi:10.1007/978-3-642-36519-5.
- 526 [34] S. W. Brenner, A.-W. Scheer, The Mathematical Theory of Finite
527 element Methods, Springer, 2008. URL: [https://doi.org/10.1007/
528 978-0-387-75934-0](https://doi.org/10.1007/978-0-387-75934-0). doi:10.1007/978-0-387-75934-0.
- 529 [35] C. Ye, E. T. Chung, Constraint energy minimizing generalized multiscale
530 finite element method for inhomogeneous boundary value problems with
531 high contrast coefficients, *Multiscale Modeling & Simulation* 21 (2023)
532 194–217.